Article

Exact Solutions of the Stochastic Conformable Broer–Kaup Equations

Humaira Yasmin [1,*], Yusuf Pandir [2], Tolga Akturk [3] and Yusuf Gurefe [4,*]

1 Department of Basic Sciences, Preparatory Year Deanship, King Faisal University, Al-Ahsa 31982, Saudi Arabia
2 Department of Mathematics, Faculty of Science and Arts, Yozgat Bozok University, 66100 Yozgat, Turkey; yusufpandir@gmail.com
3 Department of Mathematics and Science Education, Faculty of Education, Ordu University, 52200 Ordu, Turkey; tolgaakturkk@gmail.com
4 Department of Mathematics, Faculty of Science, Mersin University, 33343 Mersin, Turkey
* Correspondence: hhassain@kfu.edu.sa (H.Y.); yusufgurefe@mersin.edu.tr (Y.G.)

Abstract: In this article, the exact solutions of the stochastic conformable Broer–Kaup equations with conformable derivatives which describe the bidirectional propagation of long waves in shallow water are obtained using the modified exponential function method and the generalized Kudryashov method. These exact solutions consist of hyperbolic, trigonometric, rational trigonometric, rational hyperbolic, and rational function solutions, respectively. This shows that the proposed methods are competent and sufficient. In addition, it is aimed to better understand the physical properties by drawing two- and three-dimensional graphics of the exact solutions according to different parameter values. When these exact solutions obtained by two different methods are compared with the solutions attained by other methods, it can be said that these two methods are competent.

Keywords: stochastic conformable Broer–Kaup equations; conformable derivative; modified exponential function method; generalized Kudryashov method; exact solutions

MSC: 35C07; 60H15

1. Introduction

Partial differential equations (PDEs), mathematical models of complex physical, biological, and engineering systems, are used in various fields. The applications of nonlinear partial differential equations (NPDEs) in various fields express their versatility and importance in helping to understand and predict the behavior of complex systems with nonlinear behavior. The nonlinear variants of such models are actually of greater importance because the analysis of what kind of response they might give to the nonlinear changes of the variables is being studied with interest by researchers. From the past to the present, such nonlinear mathematical models have been used by researchers as analytical, semi-analytical, numerical, wave, etc. There are various effective methods or techniques in the literature for obtaining solutions and examining the behavior of these models. Some of these were seen as a result of the literature review as follows: the homotopy perturbation method and homotopy analysis method [1]; Adomian decomposition method [2]; the shifted Chebyshev tau method [3]; semi-analytical method [4]; analytical method [5,6]; generalized Kudryashov method [7]; sine-Gordon expansion method [8]; Jacobi elliptic function expansion method [9]; the hyperbolic trigonometric functions methods [10]; exp-function method [11]; modified extended tanh-function method [12]; new function method [13]; and modified exponential function method [14–16].

Until the middle of the 20th century, deterministic models were used effectively in various engineering problems. Considering the fact that most natural events are not

deterministic, the fractional order equations defined on the fractional derivatives and integrals are tried to be modeled to be used instead of the integer order equations. On the other hand, it has also emerged that in the mathematical modeling of many natural phenomena, the traveling waves and the fractional derivatives in random situations should be considered together [17]. The stochastic equations, which is the model used in this study, are used in a variety of fields including physics, engineering, finance, biology, and more, just like NPDEs. However, the stochastic equations can be difficult to solve due to the presence of random equations, and researchers often use numerical methods and statistical techniques to derive approximate solutions and to comment on the behavior of modeled systems. In this study, we investigated the exact solutions of an equation with a stochastic fractional derivative. In this case, we also search for stochastic conformable Broer-Kaup equations for a better understanding of random wave states [18]:

$$du + [2\,u\,D_x^\alpha u + D_x^\alpha v]dt = \sigma\,u\,d\Psi, \tag{1}$$

$$dv + [D_x^\alpha(uv) + D_x^\alpha u + D_{xxx}^\alpha u]dt = \sigma\,v\,d\Psi, \tag{2}$$

where the horizontal velocity field is denoted by $u(x,t)$; $v(x,t)$ is the height of the fluid deviating from the equilibrium position; D^α is the conformable derivative; $\Psi(t)$ is a standard Wiener process (SWP); and σ is the noise strength.

The main template of this study can be stated as follows: In the second section, information about the definition and properties of the conformable derivative is given. The third section introduces the modified exponential function method in detail. The fourth section gives detailed information about the generalized Kudryashov method. In the fifth section, the analysis of the nonlinear conformable mathematical model with the methods is given. In the last section, conclusions and comments, including all the outputs presented in this study, are given.

2. Definition and Features of Conformable Derivative

Definition 1. *The definition of the conformable derivative is given as follows [19]:*

$$D_t^\alpha\{g(t)\} = \lim_{\varepsilon \to 0} \frac{g\left(t + \varepsilon t^{1-\alpha}\right) - g(t)}{\varepsilon}. \tag{3}$$

In this study, the preferred mathematical model has been preferred because it provides some features of the basic derivative rules. Accordingly, the salient features of the appropriate derivative are as follows:

- Let functions $h \neq 0$ and g that are differentiable with respect to α be in the range $\alpha \in (0,1]$. Hence, the equation that can satisfy all real numbers e, r is as follows:

$$D_x^\alpha\{e\,g(x) + r\,h(x)\} = eD_x^\alpha\{g(x)\} + rD_x^\alpha\{h(x)\}. \tag{4}$$

- p is any constant providing the following equation:

$$D_x^\alpha\{p\} = 0. \tag{5}$$

-

$$D_x^\alpha\{g(x)h(x)\} = h(x)D_x^\alpha\{g(x)\} + g(x)D_x^\alpha\{h(x)\}. \tag{6}$$

-

$$D_x^\alpha\left\{\frac{g(x)}{h(x)}\right\} = \frac{h(x)D_x^\alpha\{g(x)\} - g(x)D_x^\alpha\{h(x)\}}{h^2(x)}. \tag{7}$$

If α is in the $(n, n + 1]$ range, the conformable derivative of g with respect to the order α is defined as

$$D_x^\alpha\{g(x)\} = \lim_{\varepsilon \to 0} \frac{g^{(\alpha-1)}\left(x + \varepsilon x^{([\alpha]-\alpha)}\right) - g^{([\alpha]-1)}(t)}{\varepsilon}. \tag{8}$$

The order α used in the above equation is the smallest integer greater than or equal to α. Also, we can use one of the newly modified versions of the derivative known as Abu-Shady–Kaabar fractional derivative [20].

3. Introduction to the Modified Exponential Function Method

Since this method is in the form of a rational function with exponential functions, it is quite easy to determine the balance procedure for any problem. Therefore, it is possible to determine whether the problem has trivial or nontrivial solutions by applying the balance procedure on this method. If the existence of nontrivial solutions is determined, it is certain to reach the hyperbolic, trigonometric, and rational wave solutions of the nonlinear problem with the help of the solution functions of the trial equation existing in this method. For these reasons, we aimed to investigate the wave solutions of this stochastic conformable problem with the modified exponential function method as well. In this section, the steps of the modified exponential function method will be introduced in detail. The general form of the dependent bivariate nonlinear conformable partial differential equation expressed by the solution function and its derivatives is as follows:

$$P(u, v, D_x^\alpha u, D_x^\alpha v, D_x^\alpha uv, D_{xxx}^\alpha u, \cdots) = 0, \tag{9}$$

where x represents space and t represents time to which the functions $u(x, t)$ and $v(x, t)$ represent the heights deviating from the equilibrium position of the fluid. The traveling wave transformation according to the independent variables in the general form of Equation (9) is as follows:

$$u(x, t) = \Phi(\xi)e^{(\sigma \Psi(t) - 1/2\sigma^2 t)}, \ v(x, t) = \Theta(\xi)e^{(\sigma \Psi(t) - 1/2\sigma^2 t)}, \ \xi = \frac{1}{\alpha}x^\alpha + \psi t, \tag{10}$$

where ψ is any constant. When Equation (10) is substituted in Equation (9), the general form of the nonlinear partial differential Equation (9) can be written as follows:

$$N\left(\Phi, \Phi^2, \Phi^3, \Phi', \Phi'', \cdots\right) = 0. \tag{11}$$

It is assumed that the solution function of Equation (11) is as follows:

$$\Phi(\xi) = \frac{\sum\limits_{j=0}^{z} A_j[e^{-\vartheta(\xi)}]^j}{\sum\limits_{i=0}^{y} B_i[e^{-\vartheta(\xi)}]^i} = \frac{A_0 + A_1 e^{-\vartheta} + \ldots + A_z e^{-z\,\vartheta}}{B_0 + B_1 e^{-\vartheta} + \ldots + B_y e^{-y\,\vartheta}}, \tag{12}$$

where A_j, B_i, $(0 \leq j \leq z, \ 0 \leq i \leq y)$ are any constants. The derivative terms required for Equation (11) are found from Equation (12). In this case, while defining the derivative of the function u with respect to ξ, the function ϑ and its derivative with respect to ϑ are needed. For this, the following equation is used:

$$\vartheta'(\xi) = e^{-\vartheta(\xi)} + \mu\, e^{\vartheta(\xi)} + \lambda. \tag{13}$$

If Equation (13) is constructed, we get the following equation:

$$\frac{e^{\vartheta(\xi)}}{\mu\, e^{2\vartheta(\xi)} + \lambda e^{\vartheta(\xi)} + 1}d\vartheta = d\xi. \tag{14}$$

If Equation (14) is integrated according to ξ, ϑ functions in the following family cases are obtained according to the values that the coefficients in the equation can take [14–16]:

Family 1: If $\mu \neq 0$ and $\lambda^2 - 4\mu > 0$,

$$\vartheta(\xi) = \ln\left[\frac{-\sqrt{\lambda^2 - 4\mu}}{2\mu}\tanh\left(\frac{\sqrt{\lambda^2 - 4\mu}}{2}(\xi + E)\right) - \frac{\lambda}{2\mu}\right]. \tag{15}$$

Family 2: If $\mu \neq 0$ and $\lambda^2 - 4\mu < 0$,

$$\vartheta(\xi) = \ln\left[\frac{\sqrt{-\lambda^2 + 4\mu}}{2\mu}\tan\left(\frac{\sqrt{-\lambda^2 + 4\mu}}{2}(\xi + E)\right) - \frac{\lambda}{2\mu}\right]. \tag{16}$$

Family 3: If $\mu = 0$, $\lambda \neq 0$ and $\lambda^2 - 4\mu > 0$,

$$\vartheta(\xi) = -\ln\left(\frac{\lambda}{e^{\lambda(\xi+E)} - 1}\right). \tag{17}$$

Family 4: If $\mu \neq 0$, $\lambda \neq 0$ and $\lambda^2 - 4\mu = 0$,

$$\vartheta(\xi) = \ln\left(-\frac{2\lambda(\xi + E) + 4}{\lambda^2(\xi + E)}\right). \tag{18}$$

Family 5: If $\mu = 0$, $\lambda = 0$ and $\lambda^2 - 4\mu = 0$,

$$\vartheta(\xi) = \ln(\xi + E), \tag{19}$$

where E, λ, μ are coefficients.

After the mathematical model in Equation (12) is defined under the conditions stated above, one of the steps to be performed is to determine the boundaries in Equation (12). For this, the balancing principle should be used. In other words, a relationship is established between y and z by balancing the highest-order nonlinear term with the highest-order nonlinear term in the nonlinear ordinary differential equation. Then, the appropriate values that will provide this correlation are determined. In this way, the boundaries of Equation (12) are determined. Then, derivative terms required in Equation (11) are obtained from Equation (12) and written in their place. There is a system of algebraic equations consisting of the coefficients in this equation. The coefficients in the $A_0, A_1, A_2, \cdots, A_z, B_0, B_1, B_2, \cdots, B_y$ form are found together with the solution of this system of equations. Then, the coefficients are substituted in Equation (12). The functions ϑ determined according to family conditions are also written in their place. It is checked whether these found functions provide the nonlinear mathematical model. Finally, the graphs simulating the physical behavior of these wave solutions satisfying the equation under appropriate parameters are obtained.

4. Introduction of the Processing Steps of the Generalized Kudryashov Method

In this section, the generalized Kudryashov method will be introduced [7]. The generalized Kudryashov method is an effective method that expands the solution functions of a trial equation to a finite series and constructs the wave solutions of the related differential equation. This method can be easily applied to the nonlinear partial differential equations; the nonlinear fractional partial differential equations; the nonlinear partial differential equations with complex coefficients; and the nonlinear stochastic equations. Also, it is clear that this method can be applied to nonintegrable equations as well as integrable ones. In this study, from this point of view, we decided to investigate the wave solutions of a nonlinear stochastic conformable differential equation via the generalized Kudryashov

method. The general form of the nonlinear conformable partial differential equation with two dependent variables is as follows:

$$P(u, v, D_x^\alpha u, D_x^\alpha v, D_x^\alpha uv, D_{xxx}^\alpha u, \cdots) = 0. \tag{20}$$

The wave transformation is given as

$$u(x, t) = \Phi(\xi)e^{(\sigma \Psi(t) - 1/2\sigma^2 t)}, \ v(x, t) = \Theta(\xi)e^{(\sigma \Psi(t) - 1/2\sigma^2 t)}, \ \xi = \frac{1}{\alpha}x^\alpha + \psi t, \tag{21}$$

where ψ is any constant. When Equation (21) is substituted in Equation (20), the general form of the nonlinear partial differential Equation (20) can be transformed into the equation

$$N\left(\Phi, \Phi^2, \Phi^3, \Phi', \Phi'', \cdots\right) = 0. \tag{22}$$

The solution function of the nonlinear conformable differential equation discussed in this article, accepted as a hypothesis, and is as follows:

$$\Phi(\xi) = \frac{\sum\limits_{j=0}^{n} a_j[Q]^j}{\sum\limits_{i=0}^{m} b_i[Q]^i} = \frac{a_0 + a_1 Q + a_2 Q^2 + \cdots + a_n Q^n}{b_0 + b_1 Q + b_2 Q^2 + \cdots + b_m Q^m}, \tag{23}$$

where $a_j, b_i, (0 \leq j \leq n, \ 0 \leq i \leq m)$ are constants. Each of the derivative terms required in Equation (22) is obtained by using Equation (23). In addition to all these cases, the following information is given about the term Q in the Φ function, which is accepted as the solution function of the mathematical model. If the equation $Q'_\xi = Q^2 - Q$ is integrated with respect to ξ, the function solution is obtained as

$$Q(\xi) = \frac{1}{1 \pm e^\xi}. \tag{24}$$

After all these calculations, the boundaries of the sum symbol in Equation (23), which is accepted as the solution function of the mathematical model, need to be determined. This process will be determined using the balancing procedure principle. In other words, a relation is established between the term containing the highest-order derivative and the nonlinear term of the highest order in the nonlinear ordinary differential equation. Accordingly, a relationship is established between m and n. Then, the appropriate parameters to achieve this equality are determined. In this case, the boundaries of Equation (23) are determined. Then, derivative terms required in Equation (22) are obtained from Equation (23) and written in their place. A system of algebraic equations consisting of the coefficients of the function in the mathematical model is established. The coefficients $a_0, a_1, a_2, \cdots, a_n$, $b_0, b_1, b_2, \cdots b_m$ are obtained by solving this system of equations. These coefficients, which are found, are written in their place in Equation (23). Finally, graphs show the behavior of the solution functions that provide the mathematical model under appropriate parameters.

5. An Application of the Modified Exponential Function Method

In this section, the modified exponential function method will be used to obtain the traveling wave solutions that provide stochastic conformable Broer–Kaup equations. If wave transform (10) is applied to Equations (1) and (2), given above as stochastic conformable Broer–Kaup equations, the following nonlinear ordinary differential equations are found:

$$\psi \Phi' + 2\Phi \Phi' + \Theta' = 0, \tag{25}$$

$$\psi \Theta' + (\Phi \Theta)' + \Phi' + \Phi''' = 0 \tag{26}$$

If Equations (25) and (26) are integrated according to ξ and the integration constants are taken as zero, we get the following equations:

$$\Theta = -\psi\,\Phi - \Phi^2, \tag{27}$$

$$\psi\,\Theta + (\Phi\,\Theta) + \Phi + \Phi'' = 0. \tag{28}$$

If Equation (27) is substituted in Equation (28), then we can find that

$$\Phi'' - \Phi^3 - 2\psi\,\Phi^2 - \left(\psi^2 - 1\right)\Phi = 0. \tag{29}$$

The balancing principle is applied to Equation (29), which is a nonlinear ordinary differential equation. For this process, by balancing the term Φ'' with the highest-order derivative in Equation (29) and the nonlinear term Φ^3 of the highest order, the following equation is obtained:

$$3z - 3y = z - y + 2 \Rightarrow z = y + 1. \tag{30}$$

For $y = 1$, we obtain $z = 2$. In this case, the solution function sought for the mathematical model according to the method is as follows:

$$\Phi(\xi) = \frac{A_0 + A_1 e^{-\vartheta} + A_2 e^{-2\,\vartheta}}{B_0 + B_1 e^{-\vartheta}}. \tag{31}$$

The derivative terms required in Equation (29) are obtained from Equation (31) and written in their place. Then, the coefficients specified in the following cases are obtained by establishing algebraic equation systems according to the powers of e^{ϑ}.

Case 1.

$$
\begin{aligned}
A_0 &= \tfrac{A_2}{24}\left(-3\sqrt{2}\,\lambda^3 + \lambda^4 + \lambda^2(4 - 8\mu) + 12\sqrt{2}\lambda\,\mu + 8\mu(1 + 2\mu)\right), \\
A_1 &= \tfrac{A_2}{4}\left(\lambda\left(4 - \sqrt{2}\lambda\right) + 4\sqrt{2}\lambda\right),\ B_0 = \tfrac{A_2}{12}\left(4 - 3\sqrt{2}\lambda + \lambda^2 - 4\mu\right), \\
B_1 &= -\tfrac{A_2}{\sqrt{2}},\ \psi = 1 - \tfrac{\lambda^2}{2} + 2\mu.
\end{aligned}
\tag{32}
$$

Substituting the above coefficients into Equation (31), we get the following wave solutions:
Family 1: when $\mu \neq 0$ and $\lambda^2 - 4\mu > 0$, then

$$u_{1,1}(x,t) = \frac{e^{\sigma\,\Psi(t) - 1/2\sigma^2 t}\left(\delta + \frac{96\mu^2}{\omega^2} + \frac{\theta}{\omega}\right)}{8 - 6\sqrt{2}\lambda + 2\lambda^2 + 2\mu\left(\frac{12\sqrt{2}}{\omega} - 4\right)}, \tag{33}$$

$$v_{1,1}(x,t) = \frac{e^{\sigma\,\Psi(t) - 1/2\sigma^2 t}\left(\delta + \frac{96\mu^2}{\omega^2} + \frac{\theta}{\omega}\right)\left(-\delta - \frac{96\mu^2}{\omega^2} - \frac{\theta}{\omega} - 2\Psi\left(4 - 3\sqrt{2}\lambda + \lambda^2 + \mu\left(\frac{12\sqrt{2}}{\omega} - 4\right)\right)\right)}{\left(16 - 12\sqrt{2}\lambda + 4\lambda^2 + 4\mu\left(\frac{12\sqrt{2}}{\omega} - 4\right)\right)^2}, \tag{34}$$

where $\xi = \frac{x^\alpha}{\alpha} + t\,\psi,\ \delta = -3\sqrt{2}\lambda^3 + \lambda^4 + \lambda^2(4 - 8\mu) + 12\sqrt{2}\lambda\,\mu + 8\mu(1 + 2\mu)$,

$$\omega = \lambda + \sqrt{\lambda^2 - 4\mu}\,\tanh\left[\frac{1}{2}\sqrt{\lambda^2 - 4\mu}(E + \xi)\right],\ \theta = 12\mu\left(\lambda\left(\sqrt{2}\lambda - 4\right) - 4\sqrt{2}\mu\right).$$

For a better understanding for the readers, the behavior of Equations (33) and (34) are graphically represented in Figures 1a and 1b, respectively.
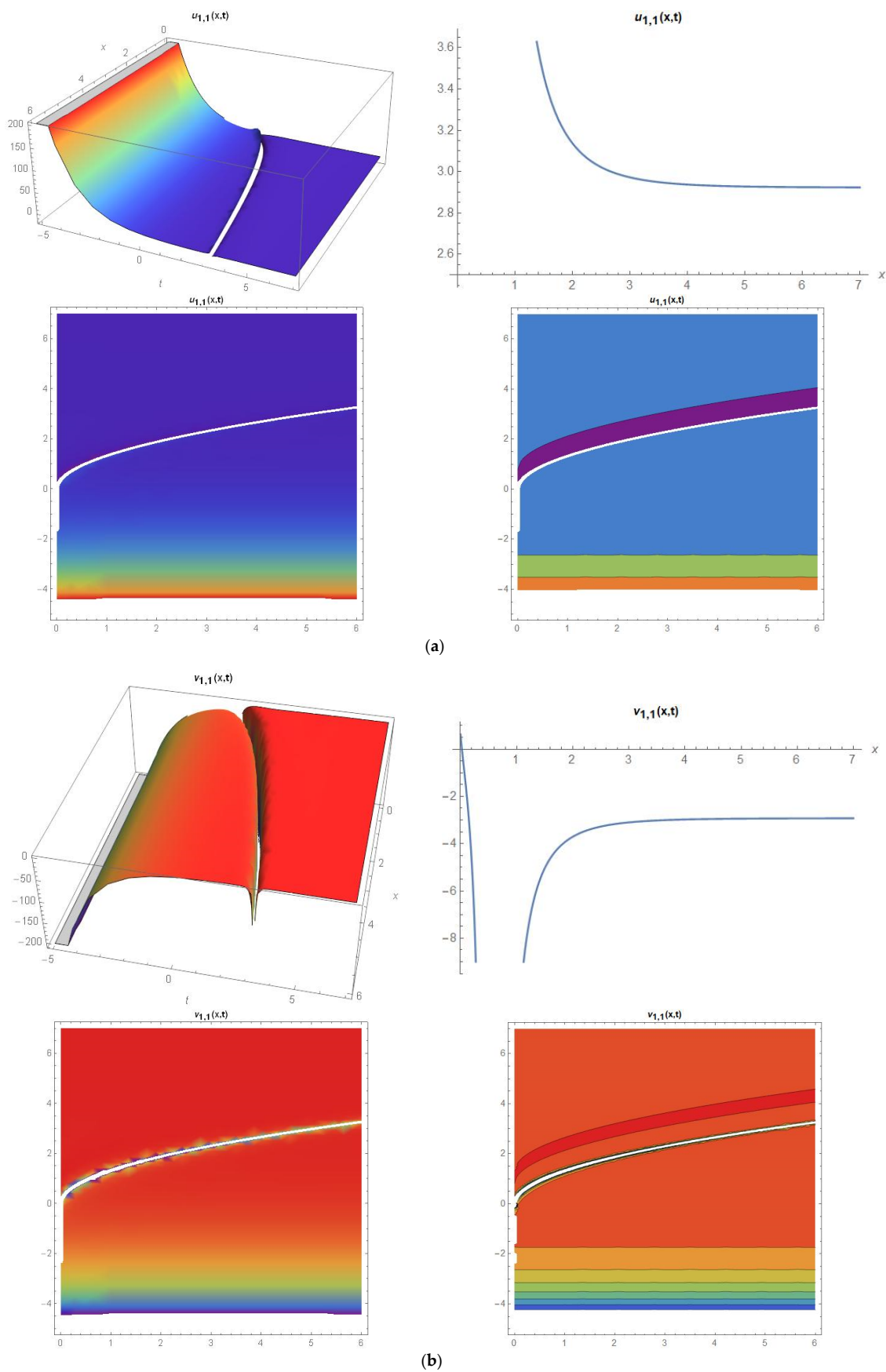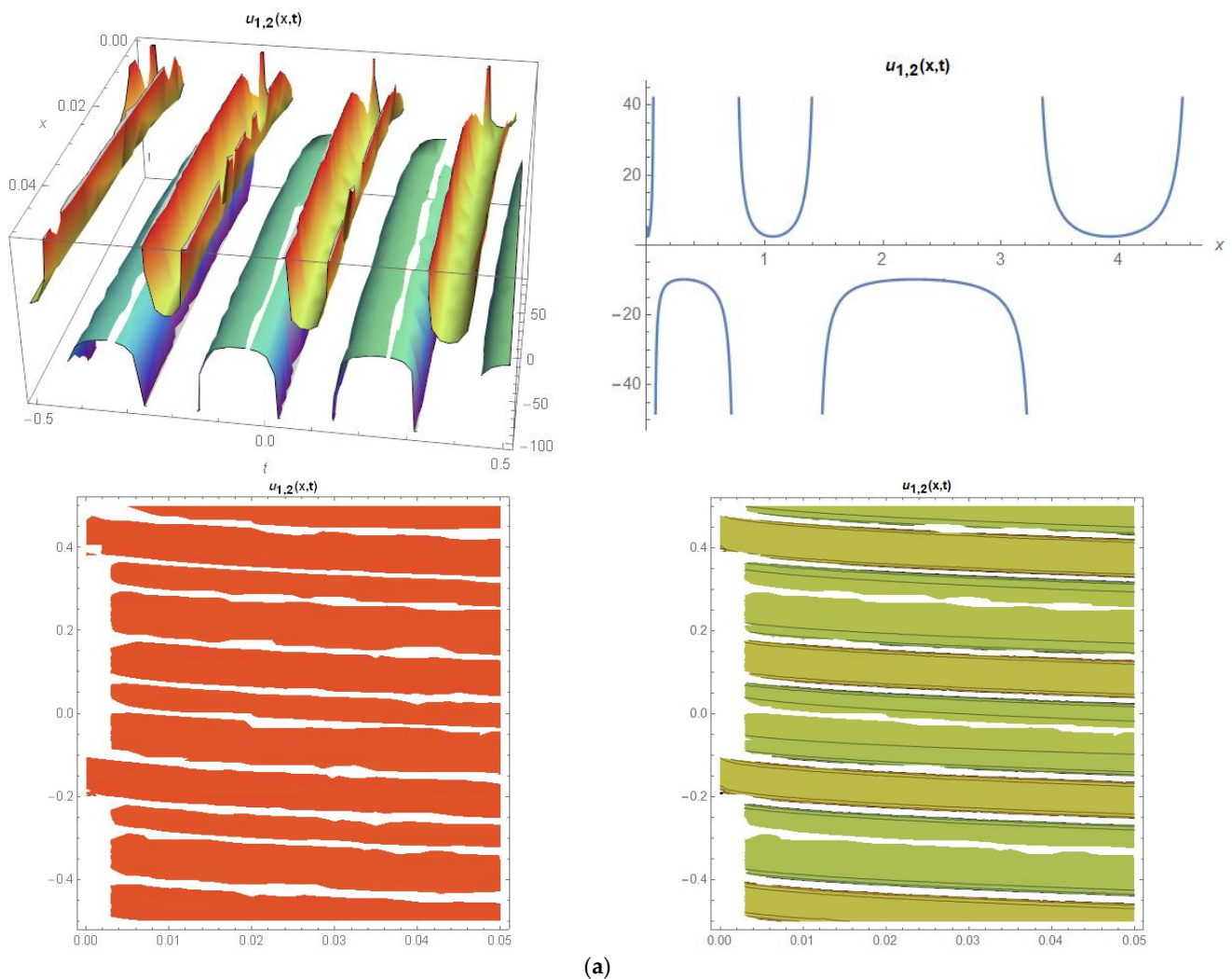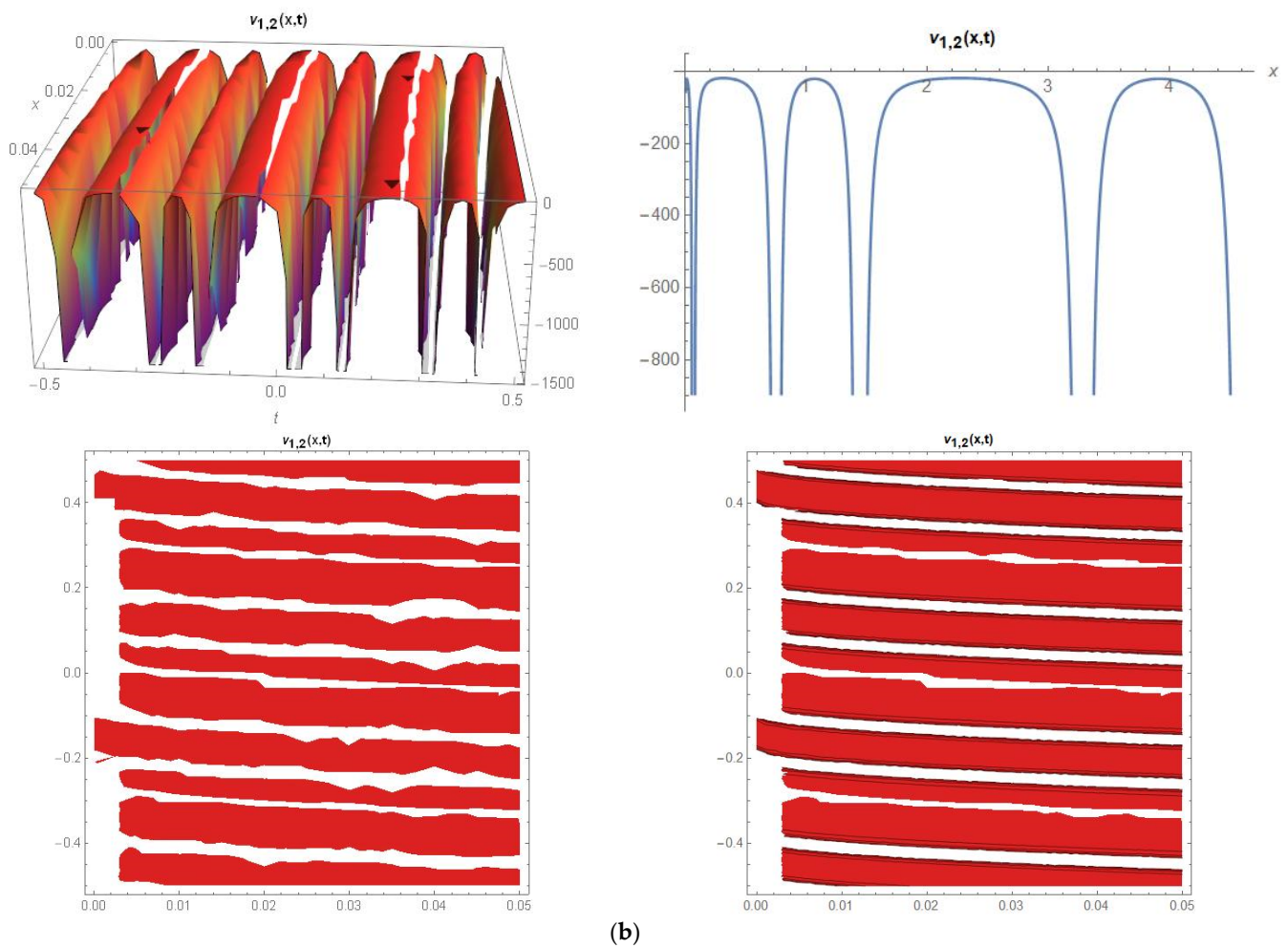
Figure 1. (**a**) Three−dimensional, two−dimensional, density, and contour graphics of Equation (33). (**b**) Three−dimensional, two−dimensional, density, and contour graphics of Equation (34).

Figure 1a,b display the behavior of Equations (33) and (34) for the values of $A_2 = 0.22$, $\mu = 1$, $\lambda = 3$, $A_0 = 0.0491369$, $A_1 = 0.271091$, $B_0 = -0.0683452$, $B_1 = -0.155563$, $\sigma = 1.25$, $\Psi = 0.75$, $\psi = -1.5$, $\alpha = 0.5$, $E = 0.75$, $t = 1$.

Family 2: when $\mu \neq 0$ and $\lambda^2 - 4\mu < 0$, then

$$u_{1,2}(x,t) = \left(\frac{e^{\sigma \Psi(t) - 1/2\sigma^2 t}\left(\delta + \frac{96\mu^2}{\phi^2} + \frac{\theta}{\phi}\right)}{8 - 6\sqrt{2}\lambda + \lambda^2 + 2\mu\left(\frac{12\sqrt{2}}{\phi} - 4\right)} \right), \tag{35}$$

$$v_{1,2}(x,t) = \left(\frac{e^{\sigma \Psi(t) - 1/2\sigma^2 t}\left(\delta + \frac{96\mu^2}{\phi^2} + \frac{\theta}{\phi}\right)\left(-\delta - \frac{96\mu^2}{(\phi)^2} - \frac{\theta}{\phi} - 2\Psi\left(4 - 3\sqrt{2}\lambda + \lambda^2 + \mu\left(\frac{12\sqrt{2}}{\phi} - 4\right)\right)\right)}{\left(16 - 12\sqrt{2}\lambda + 4\lambda^2 + 4\left(\frac{12\sqrt{2}}{\phi} - 4\right)\right)^2} \right), \tag{36}$$

where $\phi = \lambda - \sqrt{4\mu - \lambda^2}\, \tan\left[\frac{(E+\xi)}{2}\sqrt{4\mu - \lambda^2}\right]$.

For a better understanding for the readers, the behavior of Equations (35) and (36) are graphically represented in Figures 2a and 2b, respectively.

Figure 2. *Cont.*

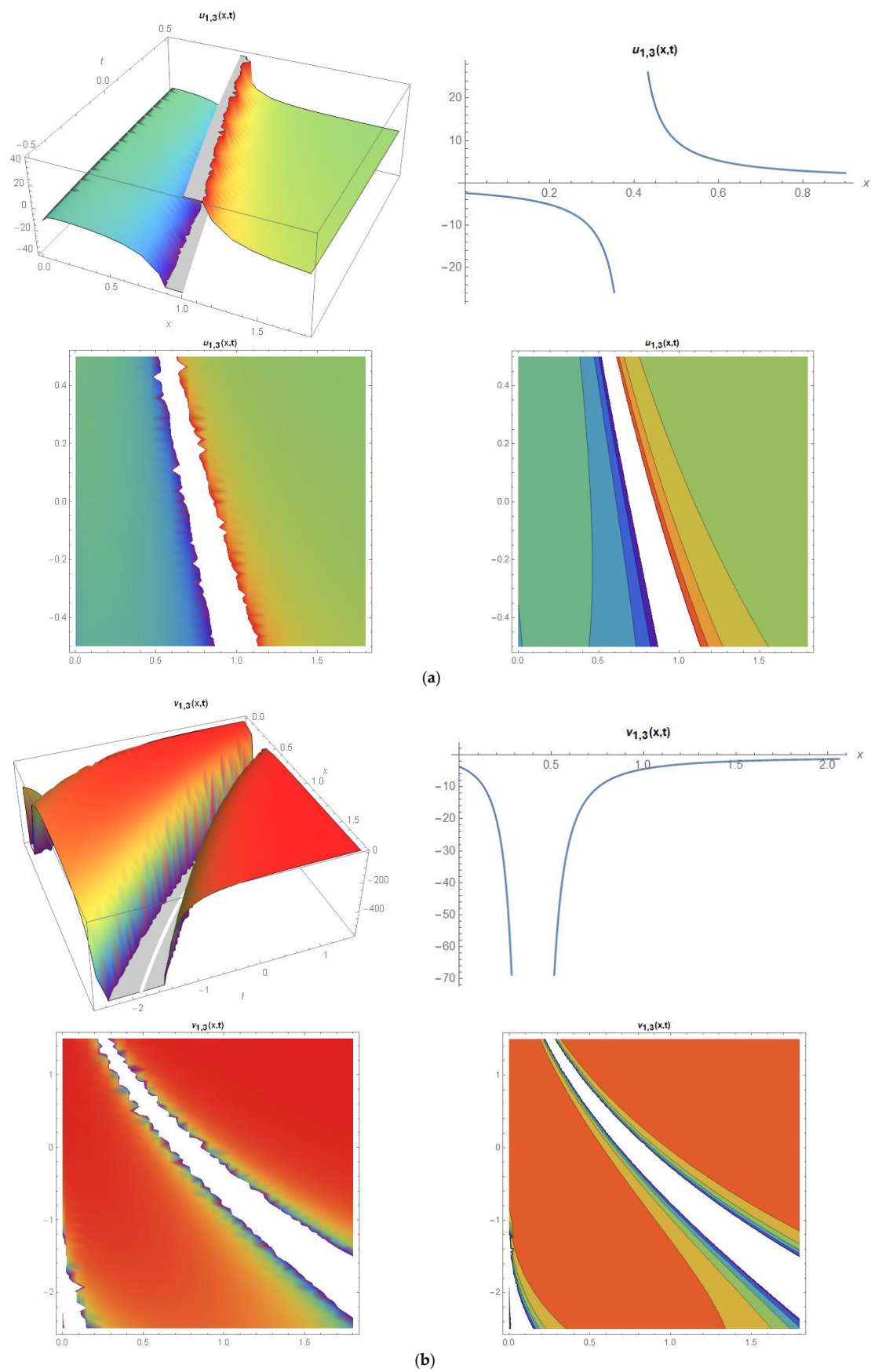**Figure 2.** (**a**) Three−dimensional, two−dimensional, density, and contour graphics of Equation (35). (**b**) Three−dimensional, two−dimensional, density, and contour graphics of Equation (36).

Figure 2a,b display the behavior of Equations (35) and (36) for the values of $A_2 = 0.22$, $\mu = 3$, $\lambda = 1$, $A_0 = 1.79363$, $A_1 = 1.0756$, $B_0 = -0.206115$, $B_1 = -0.155563$, $\sigma = 1.25$, $\Psi = 0.75$, $\psi = 6.5$, $\alpha = 0.5$, $E = 0.75$, $t = 1$.

Family 3: when $\mu = 0$, $\lambda \neq 0$ and $\lambda^2 - 4\mu > 0$, then

$$u_{1,3}(x,t) = \frac{\lambda}{2} e^{\sigma \Psi(t) - 1/2\sigma^2 t} \left(\lambda - \frac{2\sqrt{2}}{e^{\lambda(E+\xi)} - 1} - \frac{2\sqrt{2}\left(4 + 3\sqrt{2}\lambda + \lambda^2\right)}{4 + 3\sqrt{2}\lambda + \lambda^2 + e^{\lambda(E+\xi)}\left(3\sqrt{2}\lambda - 4 - \lambda^2\right)} \right), \tag{37}$$

$$v_{1,3}(x,t) = -\frac{e^{\sigma \Psi(t) - 1/2\sigma^2 t + \lambda(E+\xi)}\lambda^2 \left(8 - \lambda^2 + \left(4+\lambda^2\right)\cosh[\lambda(E+\xi)] - 3\sqrt{2}\lambda\sinh[\lambda(E+\xi)]\right)\left(\left(4+\lambda^2\right)\left(\lambda^2+2\psi\right) + \frac{3\lambda\left(4\lambda - \sqrt{2}\left(\lambda^2+2\psi\right)\sinh[\lambda(E+\xi)]\right)}{\cosh[\lambda(E+\xi)]-1}\right)}{2\left(4 + 3\sqrt{2}\lambda + \lambda^2 + e^{\lambda(E+\xi)}\left(3\sqrt{2}\lambda - 4 - \lambda^2\right)\right)^2}. \tag{38}$$

The behavior of Equations (37) and (38) are graphically represented in Figures 3a and 3b, respectively.

Figure 3. (**a**) Three−dimensional, two−dimensional, density, and contour graphics of Equation (37). (**b**) Three−dimensional, two−dimensional, density, and contour graphics of Equation (38).

Figure 3a,b display the behavior of Equations (37) and (38) for the values of $A_2 = 0.22$, $\mu = 0$, $\lambda = 1$, $A_0 = 0.00694246$, $A_1 = 0.142218$, $B_0 = 0.0138849$, $B_1 = -0.155563$, $\sigma = 1.25$, $\Psi = 0.75$, $\psi = 0.5$, $\alpha = 0.5$, $E = 0.75$, $t = 1$.

Family 4: when $\mu \neq 0$, $\lambda \neq 0$ and $\lambda^2 - 4\mu = 0$, then

$$u_{1,4}(x,t) = \frac{e^{\sigma\,\Psi(t) - 1/2\sigma^2 t}\left(\delta + \frac{6\lambda^4(E+\xi)^2}{(2+\lambda(E+\xi))^2} + \frac{3\lambda^2(E+\xi)\left(\lambda\left(\sqrt{2}\lambda - 4\right) - 4\sqrt{2}\mu\right)}{2+\lambda(E+\xi)}\right)}{8 + 2\lambda^2 - 8\mu - \frac{12\sqrt{2}\lambda}{2+\lambda(E+\xi)}}, \tag{39}$$

$$v_{1,4}(x,t) = \frac{e^{\sigma\,\Psi(t) - 1/2\sigma^2 t}\left(\delta + \kappa + \frac{6\lambda^4(E+\xi)^2}{(2+\lambda(E+\xi))^2}\right)\left(-\delta - \kappa - \frac{6\lambda^4(E+\xi)^2}{(2+\lambda(E+\xi))^2} - 2\psi\left(4 + \lambda^2 - 4\mu - \frac{6\sqrt{2}\lambda}{2+\lambda(E+\xi)}\right)\right)}{4\left(4 + \lambda^2 - 4\mu - \frac{6\sqrt{2}\lambda}{2+\lambda(E+\xi)}\right)^2}, \tag{40}$$

where $\kappa = \frac{3\lambda^2\left(\lambda\left(\sqrt{2}\lambda - 4\right) - 4\sqrt{2}\mu\right)(E+\xi)}{2+\lambda(E+\xi)}$.

The behavior of Equations (39) and (40) are graphically represented in Figures 4a and 4b, respectively.
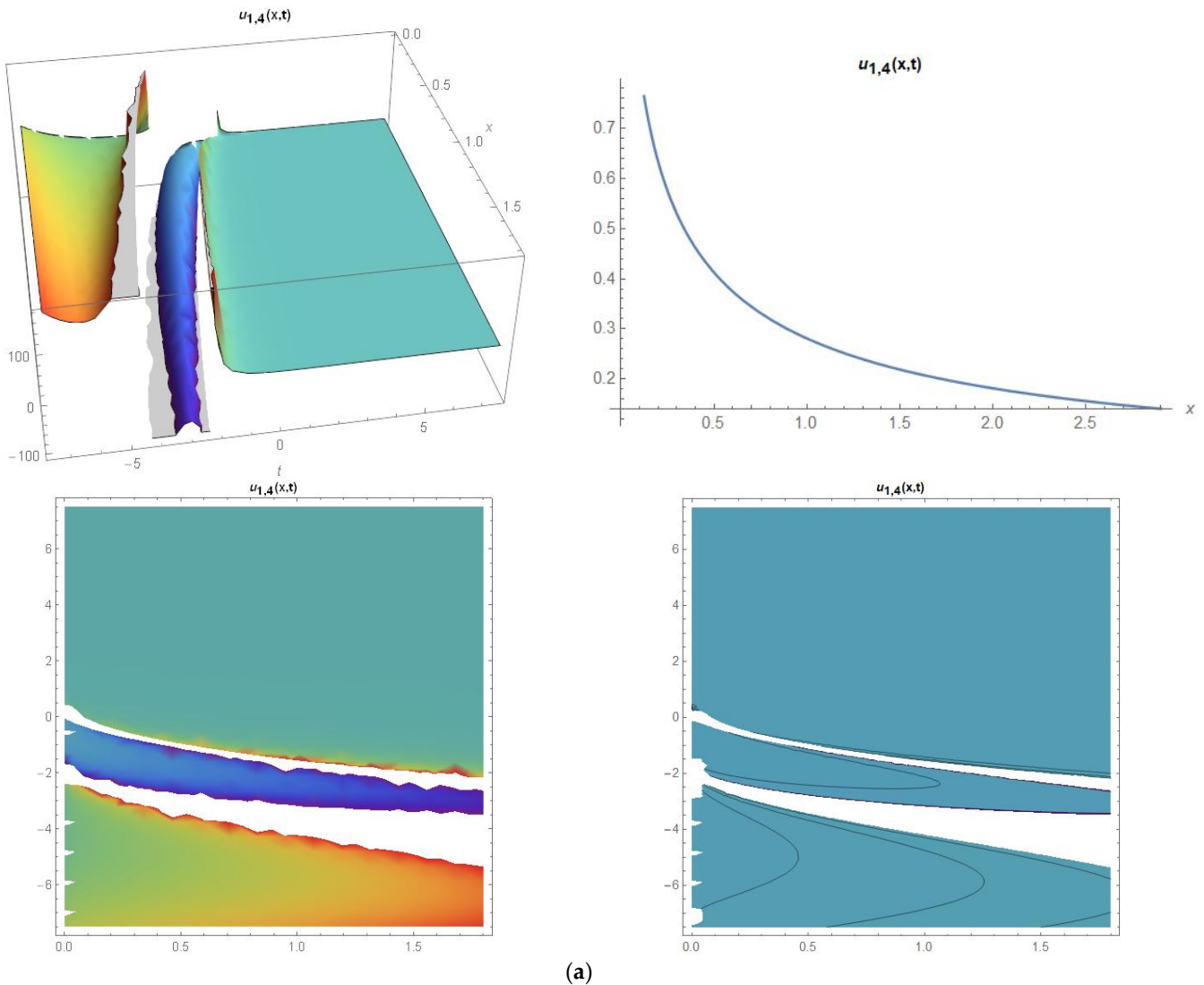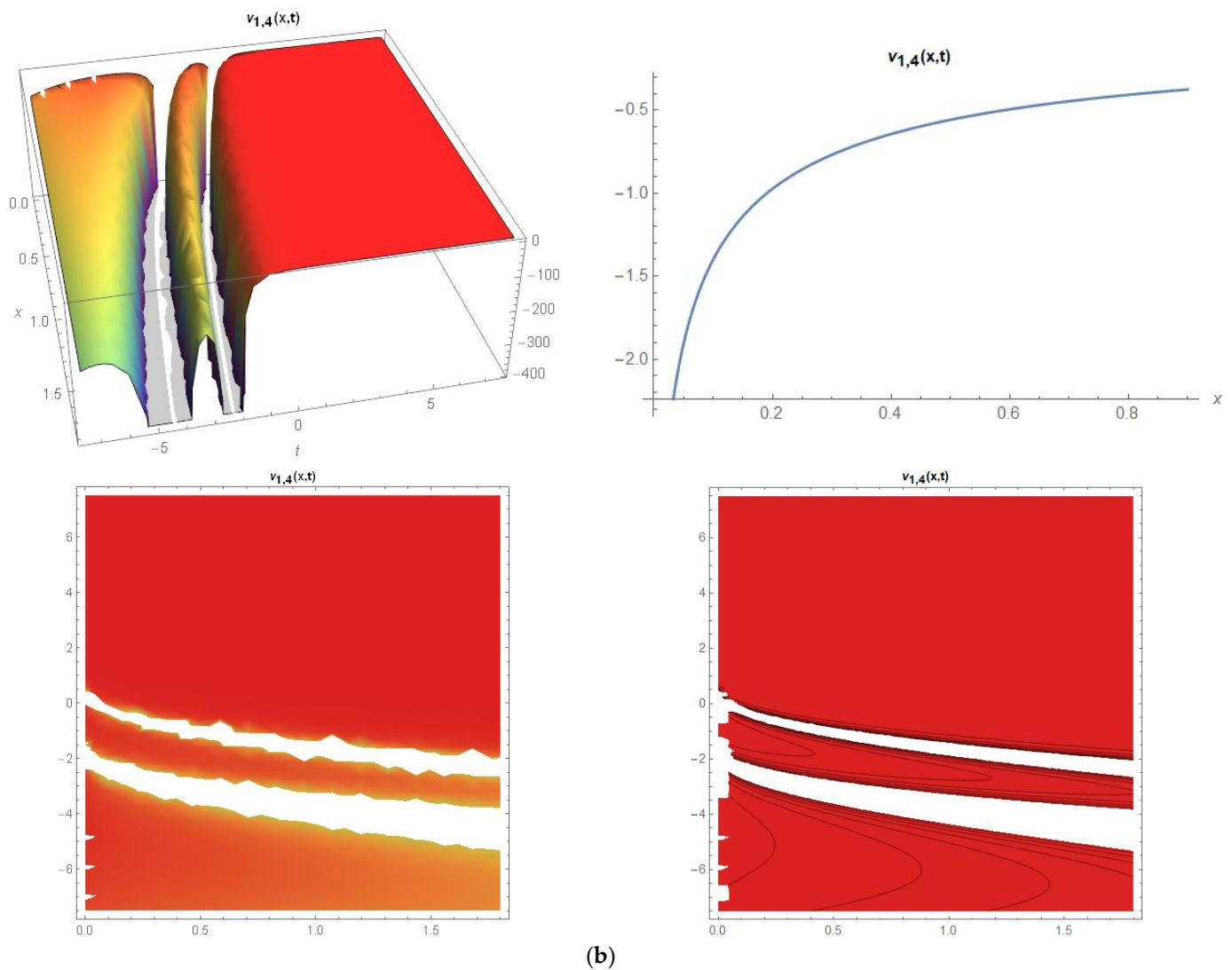

Figure 4. *Cont.*

Figure 4. (**a**) Three−dimensional, two−dimensional, density, and contour graphics of Equation (39). (**b**) Three−dimensional, two−dimensional, density, and contour graphics of Equation (40).
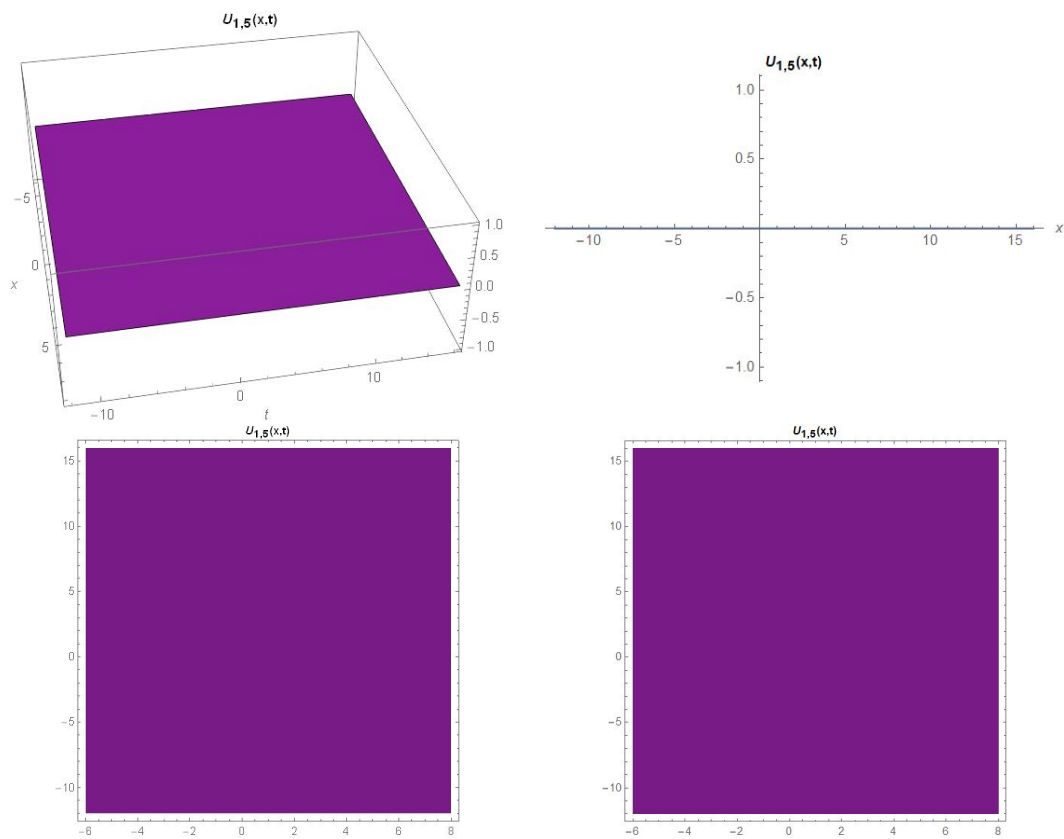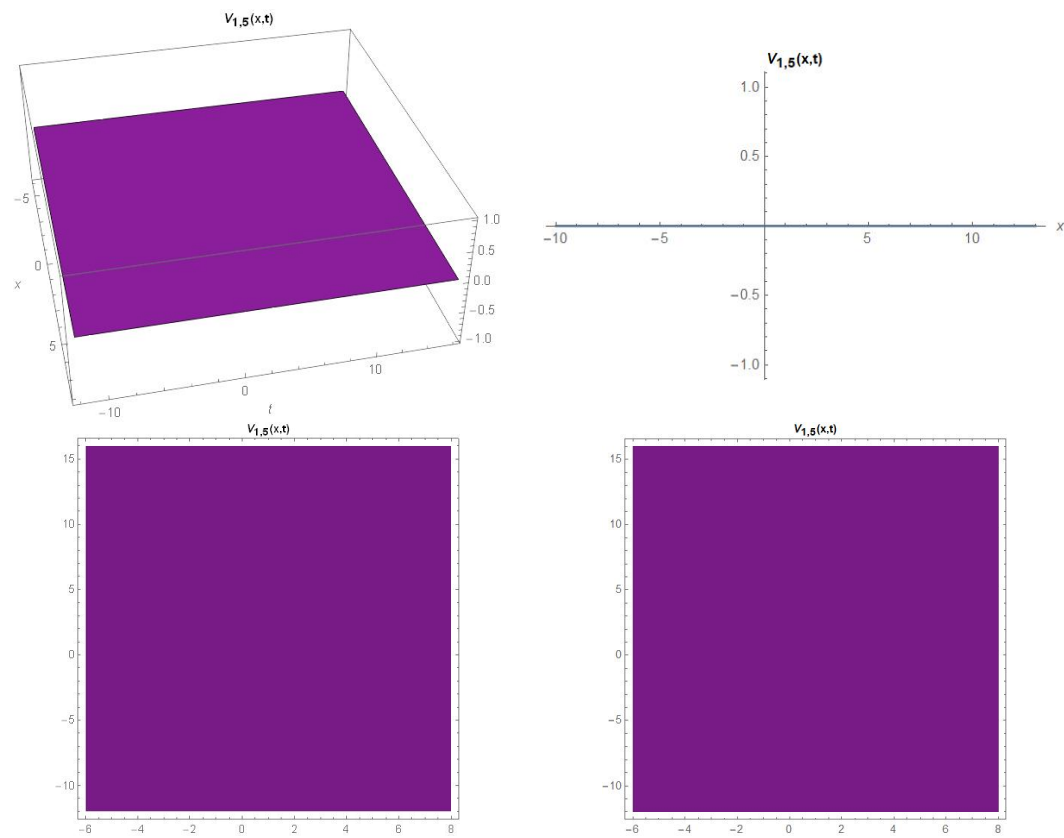
Figure 4a,b display the behavior of Equations (39) and (40) for the values of $A_2 = 0.22$, $\mu = 1$, $\lambda = 2$, $A_0 = 0.22$, $A_1 = 0.44$, $B_0 = -0.0822302$, $B_1 = -0.155563$, $\sigma = 1.25$, $\Psi = 0.75$, $\psi = 1$, $\alpha = 0.5$, $E = 0.75$, $t = 1$.

Family 5: when $\mu = 0$, $\lambda = 0$ and $\lambda^2 - 4\mu = 0$, then

$$u_{1,5}(x,t) = \left(\frac{e^{\sigma\,\Psi(t) - 1/2\sigma^2 t}\left(\delta + \frac{6\lambda^4(E+\xi)^2}{(2+\lambda(E+\xi))^2} + \frac{3\lambda^2\left(\lambda\left(\sqrt{2}\lambda - 4\right) - 4\sqrt{2}\mu\right)(E+\xi)}{2+\lambda(E+\xi)} \right)}{8 + 2\lambda^2 - 8\mu - \frac{12\sqrt{2}\lambda}{2+\lambda(E+\xi)}} \right), \qquad (41)$$

$$v_{1,5}(x,t) = \frac{e^{\sigma\,\Psi(t) - 1/2\sigma^2 t}\left(\delta + \kappa + \frac{6\lambda^4(E+\xi)^2}{(2+\lambda(E+\xi))^2} \right)\left(\delta - \kappa - \frac{6\lambda^4(E+\xi)^2}{(2+\lambda(E+\xi))^2} - 2\psi\left(4 + \lambda^2 - 4\mu - \frac{6\sqrt{2}\lambda}{2+\lambda(E+\xi)} \right) \right)}{4\left(4 + \lambda^2 - 4\mu - \frac{6\sqrt{2}\lambda}{2+\lambda(E+\xi)} \right)^2}, \qquad (42)$$

The behavior of Equations (41) and (42) are graphically represented in Figures 5a and 5b, respectively.

Figure 5. (**a**) Three−dimensional, two−dimensional, density, and contour graphics of Equation (41). (**b**) Three−dimensional, two−dimensional, density, and contour graphics of Equation (42).

Figure 5a,b display the behavior of Equations (41) and (42) for the values of $A_2 = 0.22$, $\mu = 0$, $\lambda = 0$, $A_0 = 0$, $A_1 = 0$, $B_0 = 0.0733333$, $B_1 = -0.155563$, $\sigma = 1.25$, $\Psi = 0.75$, $\psi = 1$, $\alpha = 0.5$, $E = 0.75$, $t = 1$.

Case 2.

$$A_0 = \mu A_2, \quad A_1 = \lambda A_2, \quad B_0 = -\frac{A_2}{6}\sqrt{4 + \frac{17\lambda^2}{2} - 16\mu - 6\sqrt{2\lambda^2(1 + \lambda^2 - 4\mu)}},$$

$$B_1 = -\frac{A_2\left(3\sqrt{2}\lambda + 4\sqrt{1 + \lambda^2 - 4\mu}\right)\sqrt{8 + 17\lambda^2 - 32\mu - 12\sqrt{2\lambda^2(1 + \lambda^2 - 4\mu)}}}{2(\lambda^2 - 8 + 32\mu)}, \quad (43)$$

$$\psi = \frac{\left(2\sqrt{2}(1 + \lambda^2 - 4\mu) + 3\lambda\sqrt{1 + \lambda^2 - 4\mu}\right)\sqrt{8 + 17\lambda^2 - 32\mu - 12\sqrt{2\lambda^2(1 + \lambda^2 - 4\mu)}}}{(\lambda^2 - 8 + 32\mu)}.$$

Let us analyze the traveling wave solutions given in the following solution families according to the above coefficients selected from the coefficient groups obtained by solving the system of algebraic equations. Substituting Equation (43) into Equations (27) and (31), we can easily write the following wave solutions. In this case, there are five different solution families that include various functions such as hyperbolic, rational, and trigonometric functions. In addition, the physical behavior of the obtained solutions was examined for some special values of the variables.

Family 1: if we take the conditions $\mu \neq 0$ and $\lambda^2 - 4\mu > 0$, the hyperbolic function solutions can be found as follows:

$$u_{2,1}(x,t) = \left(\frac{12e^{\sigma\Psi(t) - 1/2\sigma^2 t}\gamma}{\sqrt{\tau}\left(\sqrt{2}A_2(\lambda^3 - 4\lambda(2 + \mu) + \varsigma) - 48\mu A_2\sqrt{1 + \lambda^2 - 4\mu}\right)}\right), \quad (44)$$

$$v_{2,1}(x,t) = \frac{e^{\sigma\Psi(t) - 1/2\sigma^2 t}\gamma A_2^2\left(-\frac{\lambda\gamma}{\tau} - (\psi(\varpi))\frac{\sqrt{2}\lambda(\lambda^3 - 4\lambda(2+\mu) + \varsigma) - 48\mu\sqrt{\lambda^2(1+\lambda^2-4\mu)}}{\sqrt{\tau}}\right)}{\rho^2\left(\sqrt{2}\lambda(\lambda^3 - 4\lambda(2+\mu) + \varsigma) - 48\mu\sqrt{\lambda^2(1+\lambda^2-4\mu)}\right)^2}, \quad (45)$$

where $\xi = \frac{x^\alpha}{\alpha} + t\psi$, $\rho = \frac{(E+\xi)\sqrt{\lambda^2 - 4\mu}}{2}$, $\varpi = \lambda + \sqrt{\lambda^2 - 4\mu}\tanh[\rho]$, $\tau = (8 + 17\lambda^2 - 32\mu) - 12\lambda\sqrt{2 + 2\lambda^2 - 8\mu}$, $\gamma = \mu(\lambda^2 - 4\mu)(\lambda^2 - 8 + 32\mu)\text{sech}[\rho]^2$, $\varsigma = \sqrt{\lambda^2 - 4\mu}(\lambda^2 - 8 + 32\mu)\tanh[\rho]$.

The behavior of Equations (44) and (45) are graphically represented in Figures 6a and 6b, respectively.

Figure 6a,b display the behavior of Equations (44) and (45) for the values of $A_2 = 0.22$, $\mu = 1$, $\lambda = 3$, $A_0 = 0.22$, $A_1 = 0.66$, $B_0 = -0.053716$, $B_1 = -0.155563$, $\sigma = 1.25$, $\Psi = 0.75$, $\psi = 2.44949$, $\alpha = 0.5$, $E = 0.75$, $t = 1$.

Family 2: when $\mu \neq 0$ and $\lambda^2 - 4\mu < 0$, then

$$u_{2,2}(x,t) = \frac{12e^{\sigma\Psi(t) - 1/2\sigma^2 t}\lambda\mu(\lambda^2 - 4\mu)(\lambda^2 - 8 + 32\mu)\sec[o]^2}{\sqrt{\tau}\left(\lambda - \sqrt{4\mu - \lambda^2}\tan[o]\right)\left(\sqrt{2}\lambda\,\Omega - 48\mu\sqrt{\lambda^2(1 + \lambda^2 - 4\mu)}\right)}, \quad (46)$$

$$v_{2,2}(x,t) = \frac{12e^{\sigma\Psi(t) - 1/2\sigma^2 t}\chi\left(\frac{12A_2\chi}{(8 + 17\lambda^2 - 32\mu) - 12\sqrt{2\lambda^2(1+\lambda^2-4\mu)}} + \frac{\lambda\psi(\phi)}{A_2\sqrt{(8 + 17\lambda^2 - 32\mu) - 12\lambda\sqrt{2+2\lambda^2-8\mu}}}\right)}{\phi^2\lambda^2}, \quad (47)$$

where $o = \frac{(E+\xi)}{2}\sqrt{4\mu - \lambda^2}$, $\lambda = \sqrt{2}\lambda A_2^2\Omega - 48A_2^2\lambda\mu\sqrt{1 + \lambda^2 - 4\mu}$, $\Omega = \left(\lambda^3 - 4\lambda(2 + \mu) - \sqrt{4\mu - \lambda^2}(\lambda^2 - 8 + 32\mu)\tan[o]\right)$, $\chi = \lambda\mu(\lambda^2 - 4\mu)(\lambda^2 - 8 + 32\mu)\text{sech}[o]^2$.
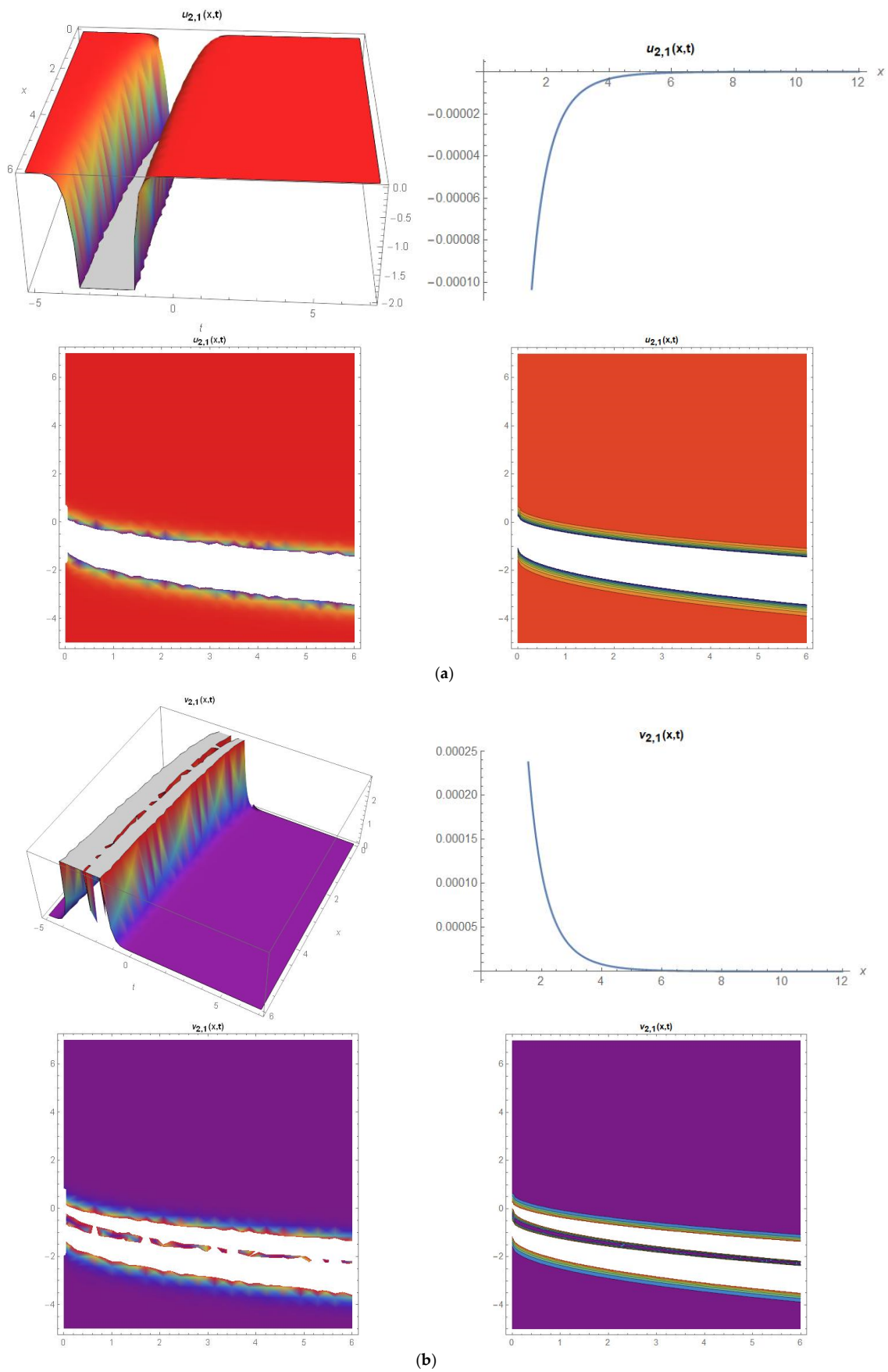
Figure 6. (**a**) Three−dimensional, two−dimensional, density, and contour graphics of Equation (44).
(**b**) Three−dimensional, two−dimensional, density, and contour graphics of Equation (45).

The behavior of real and imaginary parts of Equations (46) and (47) are graphically represented in Figure 7a–d.
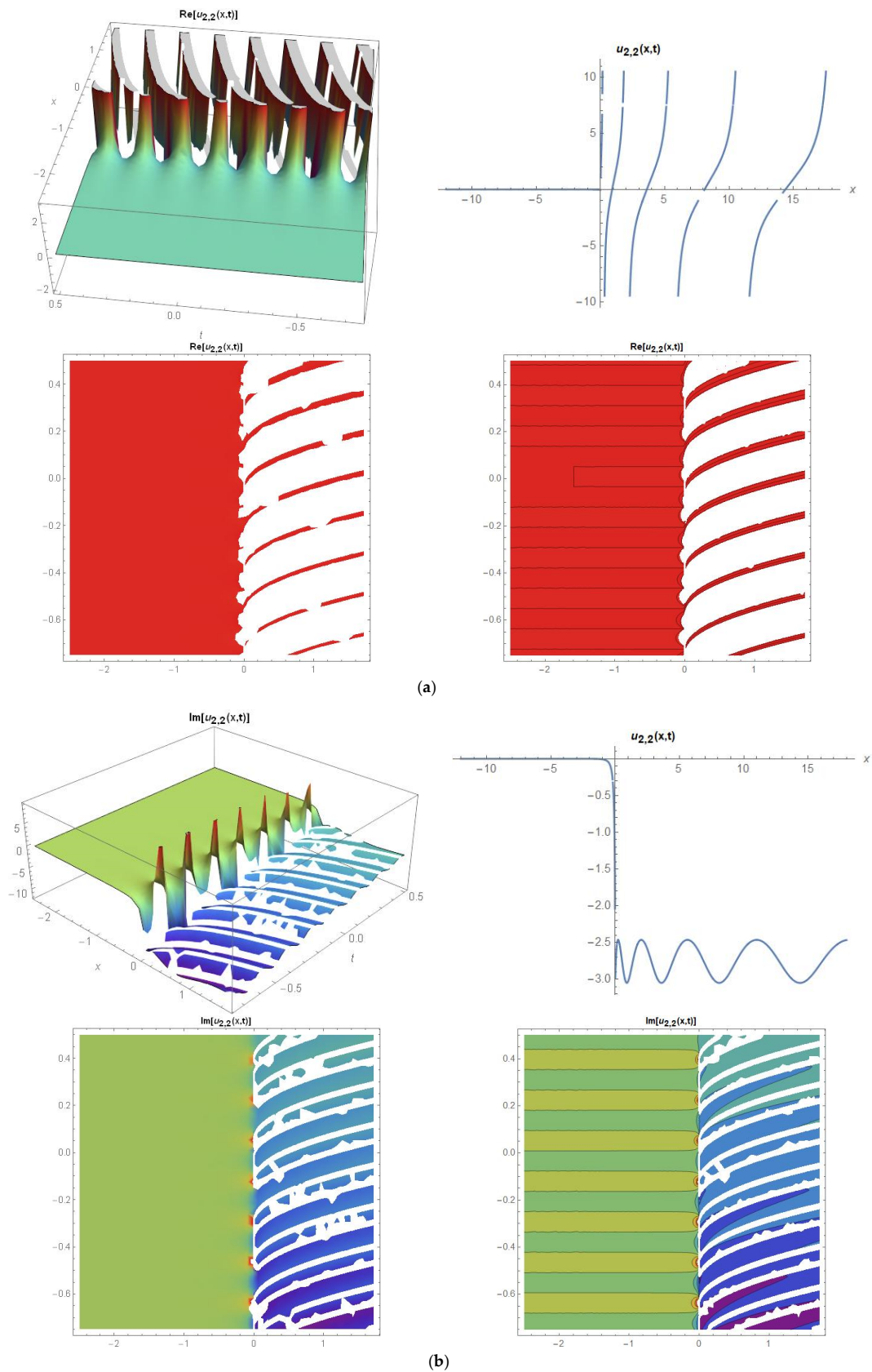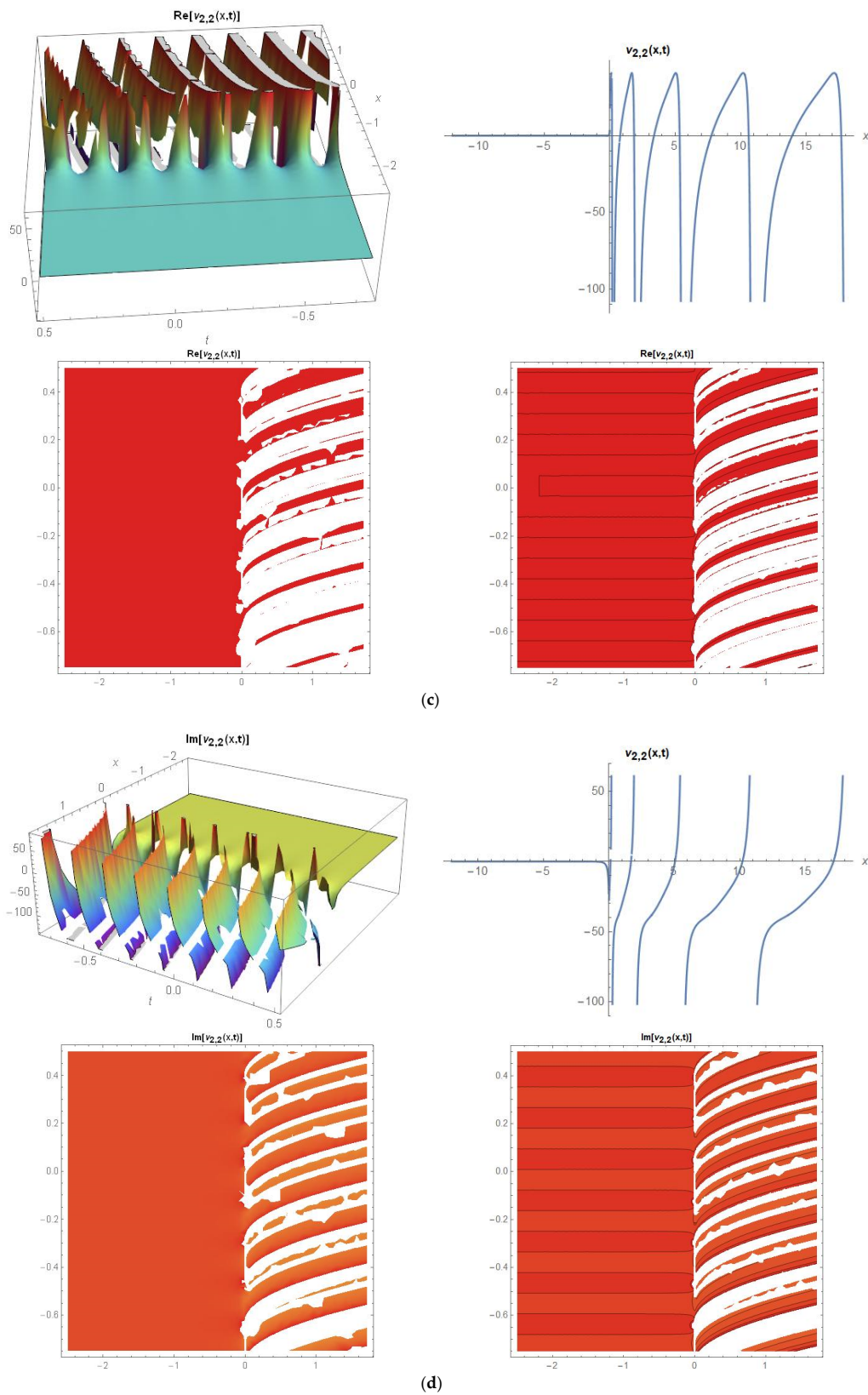

(**a**)

(**b**)

Figure 7. *Cont.*

(c)

(d)

Figure 7. (**a**) Three−dimensional, two−dimensional, density, and contour graphics for the real part of Equation (46). (**b**) Three−dimensional, two−dimensional, density, and contour graphics for the imaginary part of Equation (46). (**c**) Three−dimensional, two−dimensional, density, and contour graphics for real part of Equation (47). (**d**) Three−dimensional, two−dimensional, density, and contour graphics for imaginary part of Equation (47).

Figure 7a–d display the behavior of Equations (46) and (47) for the values $A_0 = 3$, $A_1 = 1$ $A_2 = 1$, $B_0 = -\frac{\sqrt{-71-24i\sqrt{5}}}{6\sqrt{2}}$, $B_1 = -\frac{\sqrt{-71-24i\sqrt{5}}\left(3\sqrt{2}+4i\sqrt{10}\right)}{178}$, $\mu = 3$, $\lambda = 1$, $\sigma = 1.25$, $\Psi = 0.75$, $\psi = -11$, $\alpha = 0.5$.

Family 3: when $\mu = 0$, $\lambda \neq 0$ and $\lambda^2 - 4\mu > 0$, then

$$u_{2,3}(x,t) = \left(-\frac{e^{(E+\xi)\lambda-1/2\sigma^2 t+\sigma\,\Psi(t)}\lambda^2\left(\lambda^2-8\right)}{\hbar(\xi)\left(e^{(E+\xi)\lambda}-1\right)}\right), \tag{48}$$

$$v_{2,3}(x,t) = e^{-1/2\sigma^2 t+\sigma\,\Psi(t)}\left(\frac{12\psi e^{2(E+\xi)\lambda}\lambda^2\left(\lambda^2-8\right)^2}{\hbar(\xi)\left(e^{(E+\xi)\lambda}-1\right)} - \frac{e^{2(E+\xi)\lambda}\lambda^4\left(\lambda^2-8\right)^2}{\sqrt{2}(\hbar(\xi))^2\left(e^{(E+\xi)\lambda}-1\right)^2}\right), \tag{49}$$

where $\hbar(\xi) = \sqrt{2}\left(8+17\lambda^2+e^{(E+\xi)\lambda}\left(\lambda^2-8\right)+24\lambda\sqrt{\lambda^2+1}\right)\sqrt{8+17\lambda^2-12\sqrt{2}\lambda\sqrt{\lambda^2+1}}$.

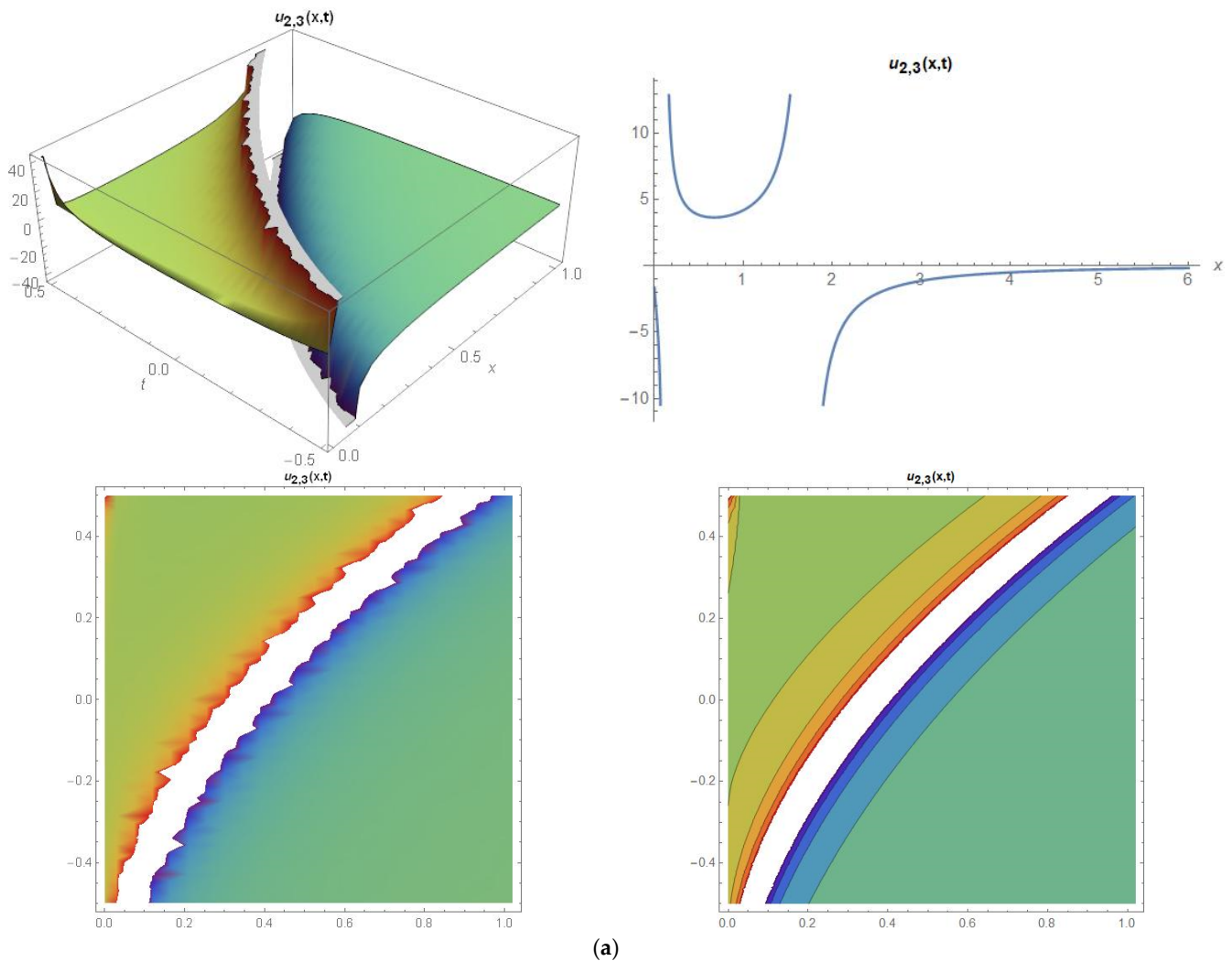The behavior of Equations (48) and (49) are graphically represented in Figures 8a and 8b, respectively.
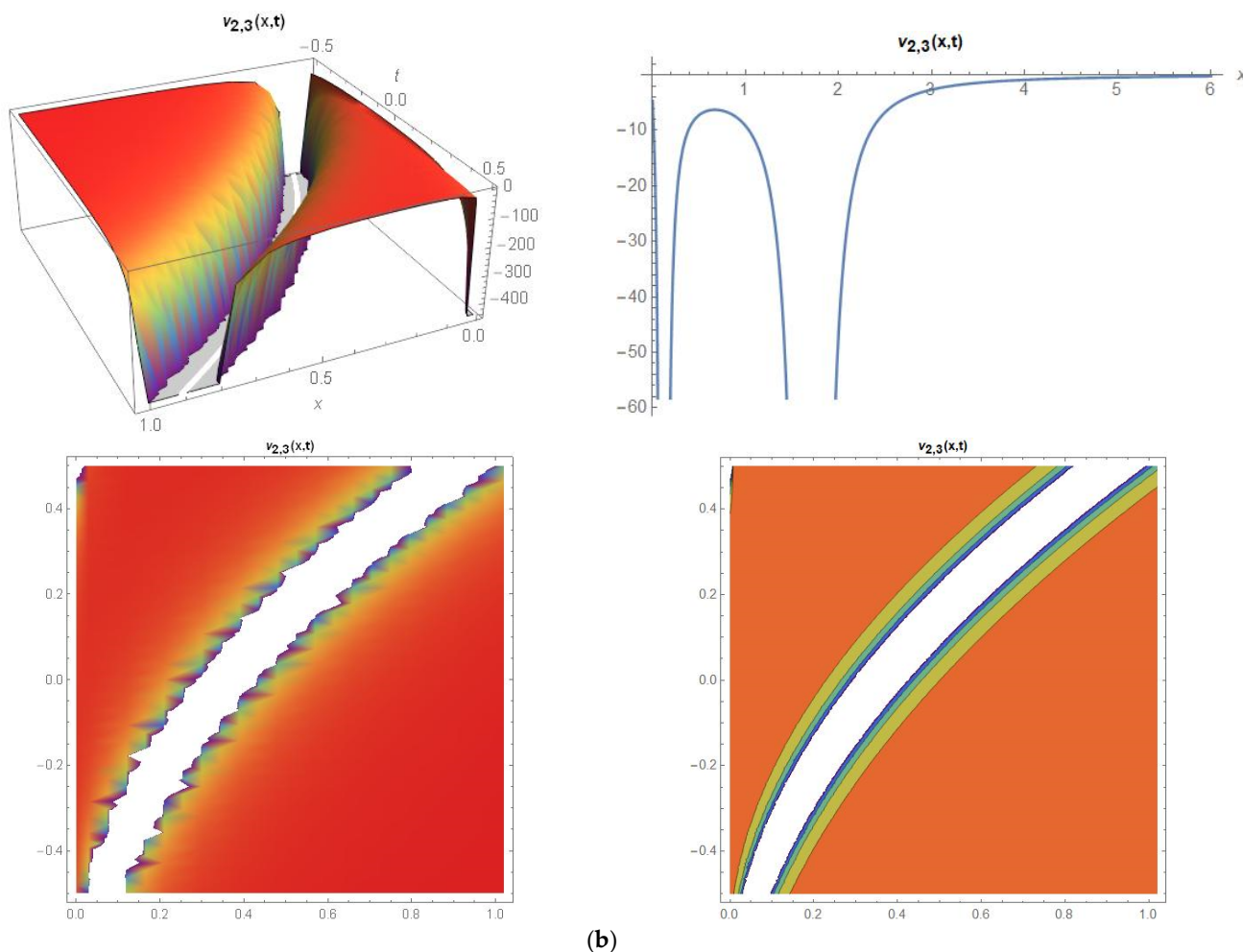

(**a**)

Figure 8. *Cont.*

Figure 8. (**a**) Three−dimensional, two−dimensional, density, and contour graphics of Equation (48).
(**b**) Three−dimensional, two−dimensional, density, and contour graphics of Equation (49).

Figure 8a,b display the behavior of Equations (48) and (49) for the values of
$A_0 = 0$, $A_1 = 1$, $A_2 = 1$, $B_0 = -\frac{1}{6\sqrt{2}}$, $B_1 = -\frac{1}{\sqrt{2}}$, $\mu = 0$, $\lambda = 1$, $\sigma = 1.25$, $\Psi = 0.75$,
$\psi = -\sqrt{2}$, $\alpha = 0.5$, $E = 0.75$, $t = 1$

Family 4: when $\mu \neq 0$, $\lambda \neq 0$ and $\lambda^2 - 4\mu = 0$, then

$$u_{2,4}(x,t) = -\frac{3e^{-1/2\sigma^2 + \sigma\Psi}\left((E+\xi)\lambda(4+(E+\xi)\lambda)(\lambda^2-4\mu)-16\mu\right)(\lambda^2-8+32\mu)}{\left(2(2+(E+\xi)\lambda)Y(\xi)\sqrt{8+17\lambda^2-32\mu-12\lambda\sqrt{2+2\lambda^2-8\mu}}\right)},$$

(50)

$$v_{2,4}(x,t) = \frac{-9\Delta^2(\lambda^2-8+32\mu)^2 e^{-1/2\sigma^2+\sigma\Psi}}{2\mho\,Y(\xi)\left(4\mho^2(Y(\xi))^2+\Delta\right)},$$

(51)

where $Y(\xi) = \sqrt{2}\Big(\big(8+\lambda(4(1+\lambda^2-4\mu)(E+\xi)-\lambda)-32\mu\big)+6(E+\xi)\lambda^2\sqrt{1+\lambda^2-4\mu}\Big)$,
$\mho = (2+(E+\xi)\lambda)^2\Big((8+17\lambda^2-32\mu)-12\lambda\sqrt{2+2^2-8\mu}\Big)$, $\Delta = (E+\xi)\lambda(4+(E+\xi)\lambda)$
$(\lambda^2-4\mu)-16\mu$.

The behavior of Equations (50) and (51) are graphically represented in Figures 9a and 9b,
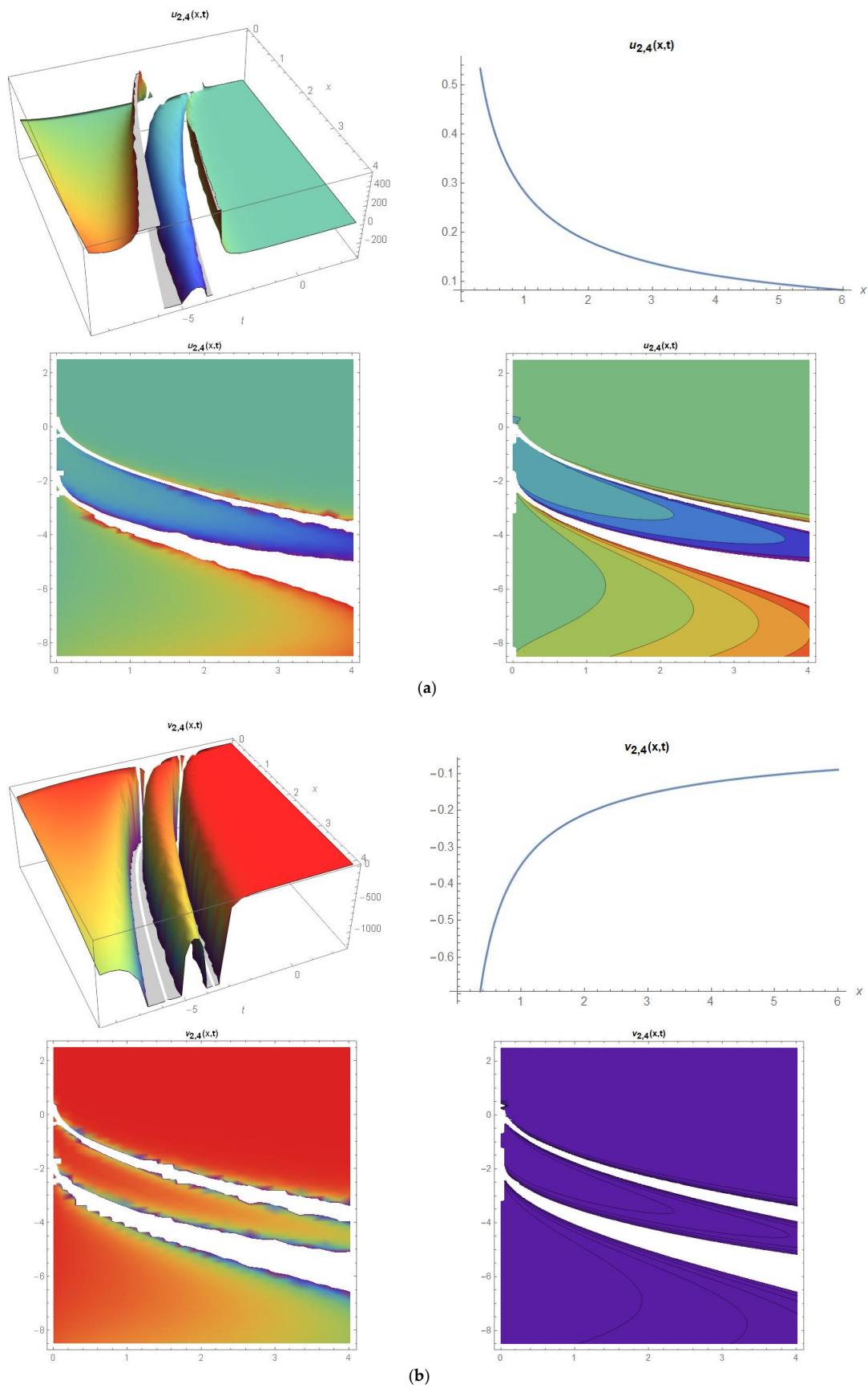respectively.

Figure 9. (**a**) Three−dimensional, two−dimensional, density, and contour graphics of Equation (50). (**b**) Three−dimensional, two−dimensional, density, and contour graphics of Equation (51).

Figure 9a,b display the behavior of Equations (50) and (51) for the values of $A_2 = \mu = A_0 = t = 1$ $\lambda = A_1 = 2$, $B_0 = -\dfrac{\sqrt{11-6\sqrt{2}}}{3\sqrt{2}}$, $B_1 = -\dfrac{\sqrt{11-6\sqrt{2}}(2+3\sqrt{2})}{14}$, $\sigma = 1.25$, $\psi = \dfrac{\sqrt{11-6\sqrt{2}}(3+\sqrt{2})}{7}$, $\alpha = 0.5$, $E = \Psi = 0.75$.

Family 5: when $\mu = 0$, $\lambda = 0$ and $\lambda^2 - 4\mu = 0$, the parameters make the solution function undefined under these conditions; no data related to any solution could be obtained.

6. Analysis of Wave Solutions of Mathematical Model with the Generalized Kudryashov Method

In this section, the generalized Kudryashov method will be used to derive traveling wave solutions that satisfy the stochastic conformable Broer–Kaup equations. In addition, since some of the operations mentioned below are the same operations with the developed exponential function method, the steps of the above equations will be mentioned.

If the wave transform (21) is applied to Equations (1) and (2) given as stochastic conformable Broer–Kaup equations, just as in the modified exponential function method, the system of nonlinear partial differential Equations (25) and (26) is transformed to a nonlinear ordinary differential equation. Then, it is reduced to the system of Equations (27) and (28) by integrating according to ζ in order to analyze the solution of this system of equations more efficiently. Equation (29) is obtained by arranging this system of equations. In this system of equations, there is a correlation between the limits of the solution function, which is considered hypothetical according to this method, by balancing the term with the highest-order derivative and the term with the highest degree. The solution function, considered as the following assumption, is obtained by giving appropriate values to the m and n parameters in the determined relation:

$$u(\xi) = \frac{\sum\limits_{j=0}^{2} a_j [Q]^j}{\sum\limits_{i=0}^{1} b_i [Q]^i} = \frac{a_0 + a_1 Q + a_2 Q^2}{b_0 + b_1 Q}, \tag{52}$$

where $a_j, b_i, (0 \leq j \leq n, 0 \leq i \leq m)$ are constants. The derivative terms required in Equation (29) are obtained from Equation (51) and written in their place. Then, this system of equations is arranged according to the powers of Q, and a system of algebraic equations is established. The unknown coefficients in the following cases are found with the solution of this system of algebraic equations. These coefficients are written in their place in the solution function, which is considered a hypothesis. With the program's help, these functions are checked in order to establish whether they provide the nonlinear ordinary differential equation first and then the nonlinear partial differential equation second. Then, the graphs simulating the behavior of these functions, which are considered the mathematical model's solution, are drawn under the appropriate parameters.

Case 1.

$$a_0 = \frac{6 + 5\sqrt{2}}{24} b_1, \ a_1 = -\frac{1 + 2\sqrt{2}}{2} b_1, \ a_2 = \sqrt{2} b_1, \ b_0 = -\frac{6 + 5\sqrt{2}}{12} b_1, \ c = -\frac{1}{2}. \tag{53}$$

According to the coefficients obtained by solving the algebraic equation system, the traveling wave solutions of the mathematical model are as follows:

$$u_{1,1}(x,t) = \frac{1}{6} e^{-1/2\sigma^2 t + \sigma \Psi(t)} \left(2 - 3\sqrt{2} \tanh\left[\frac{\zeta}{2}\right] - \frac{7\cosh\left[\frac{\zeta}{2}\right]}{\wp(\xi)} \right), \tag{54}$$

$$v_{1,1}(x,t) = \frac{e^{-1/2\sigma^2 t+\sigma\,\Psi(t)}\mathrm{sech}^2\left[\frac{\xi}{2}\right](\wp(\xi)-7)((2\psi-1)\wp(\xi)+10\psi+7)}{16\left(\wp(\xi)\right)^2}, \tag{55}$$

where $\wp(\xi) = 5\cosh\left[\frac{\xi}{2}\right] + 3\sqrt{2}\sinh\left[\frac{\xi}{2}\right]$.

The behavior of Equations (54) and (55) are graphically represented in Figures 10a and 10b, respectively.
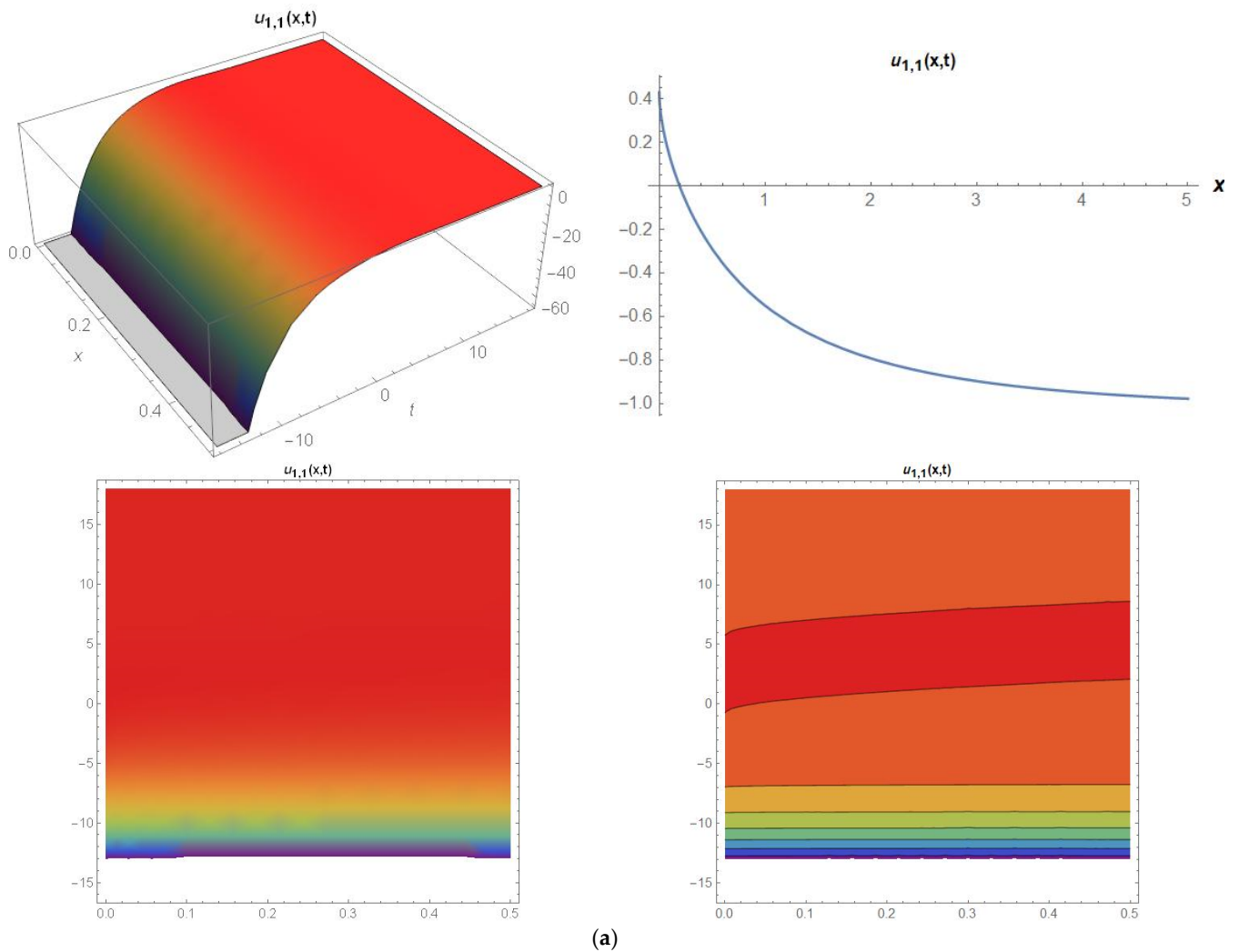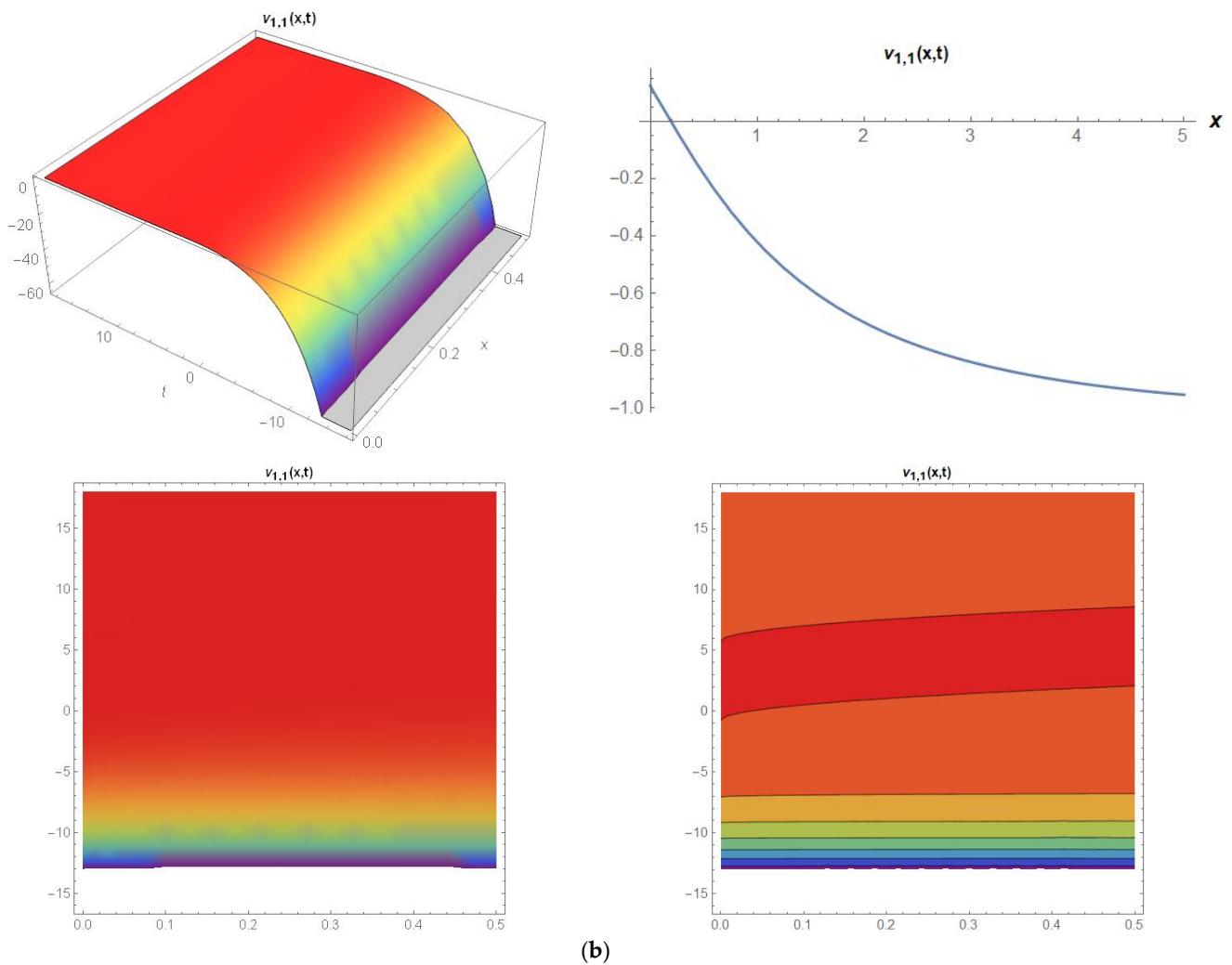

Figure 10. *Cont.*

Figure 10. (**a**) Three−dimensional, two−dimensional, density, and contour graphics of Equation (54). (**b**) Three−dimensional, two−dimensional, density, and contour graphics of Equation (55).

Figure 10a,b display the behavior of Equations (54) and (55) for the values of $a_0 = -0.413917, a_1 = 1.4548, a_2 = -1.0748, b_0 = 0.827834, b_1 = -0.76, \psi = -0.5, \sigma = 0.77, \Psi = 1.32, \alpha = 0.5, t = 1$.

$$u_{1,2}(x,t) = \frac{1}{6}e^{-1/2\sigma^2 t + \sigma\Psi(t)}\left(2 - 3\sqrt{2}\coth\left[\frac{\xi}{2}\right] - \frac{7}{5 + 3\sqrt{2}\coth\left[\frac{\xi}{2}\right]}\right), \tag{56}$$

$$v_{1,2}(x,t) = \frac{e^{-1/2\sigma^2 t + \sigma\Psi(t)}\operatorname{csch}^2\left[\frac{\xi}{2}\right](7 + \wp(\xi))((2\psi - 1)\wp(\xi) - 10\psi - 7)}{16(\Im(\xi))^2}, \tag{57}$$

where $\wp(\xi) = 5\cosh\left[\frac{\xi}{2}\right] + 3\sqrt{2}\sinh\left[\frac{\xi}{2}\right]$, $\Im(\xi) = 5\sinh\left[\frac{\xi}{2}\right] + 3\sqrt{2}\cosh\left[\frac{\xi}{2}\right]$.

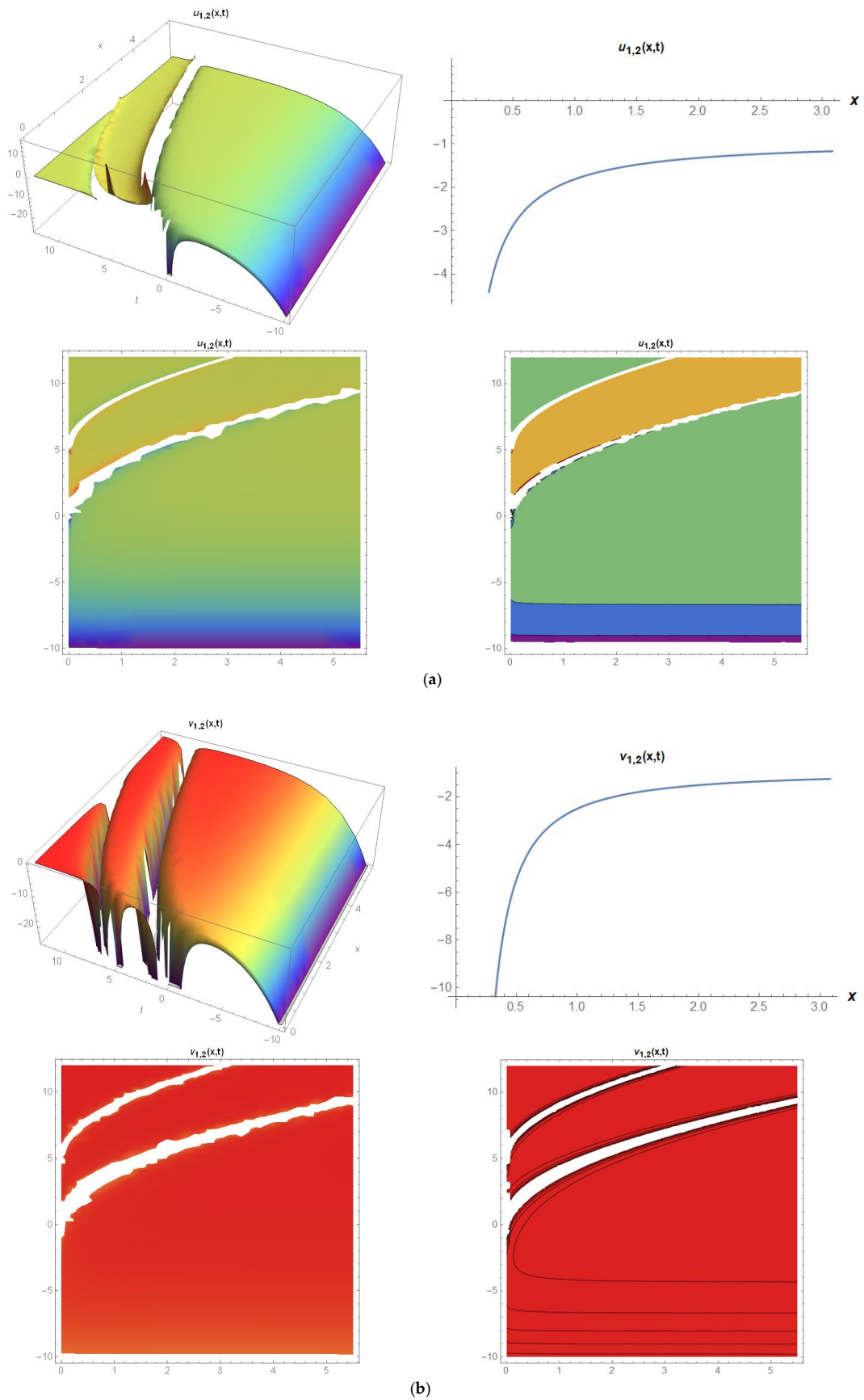The behavior of Equations (56) and (57) are graphically represented in Figures 11a and 11b, respectively.

Figure 11. (**a**) Three−dimensional, two−dimensional, density, and contour graphics of Equation (56). (**b**) Three−dimensional, two−dimensional, density, and contour graphics of Equation (57).

Figure 11a,b display the behavior of Equations (56) and (57) for the values of $a_0 = -0.413917$ $a_1 = 1.4548$, $a_2 = -1.0748$, $b_0 = 0.827834$, $b_1 = -0.76$, $\psi = -0.5$, $\sigma = 0.77$, $\Psi = 1.32$, $\alpha = 0.5$, $t = 1$.

Case 2.

$$a_0 = 0,\ a_1 = -\sqrt{2}b_1,\ a_2 = \sqrt{2}b_1,\ ,b_0 = -\frac{7b_1}{6},\ c = -\sqrt{2}. \tag{58}$$

According to the coefficients obtained from the system of algebraic equations, the traveling wave solutions of the model can be written as

$$u_{2,1}(x,t) = \frac{3\sqrt{2}\,e^{-1/2\sigma^2 t + \sigma\,\Psi(t)}}{\Lambda(\xi)}, \tag{59}$$

$$v_{2,1}(x,t) = \frac{3e^{-1/2\sigma^2 t + \sigma\,\Psi(t)}\left(-6 - \sqrt{2}\,\psi\,\Lambda(\xi)\right)}{\left(\Lambda(\xi)\right)^2}, \tag{60}$$

where $\Lambda(\xi) = 4 + 4\cosh[\xi] + 3\sinh[\xi]$.

For a better understanding for the readers, the behavior of Equations (59) and (60) are graphically represented in Figures 12a and 12b, respectively.
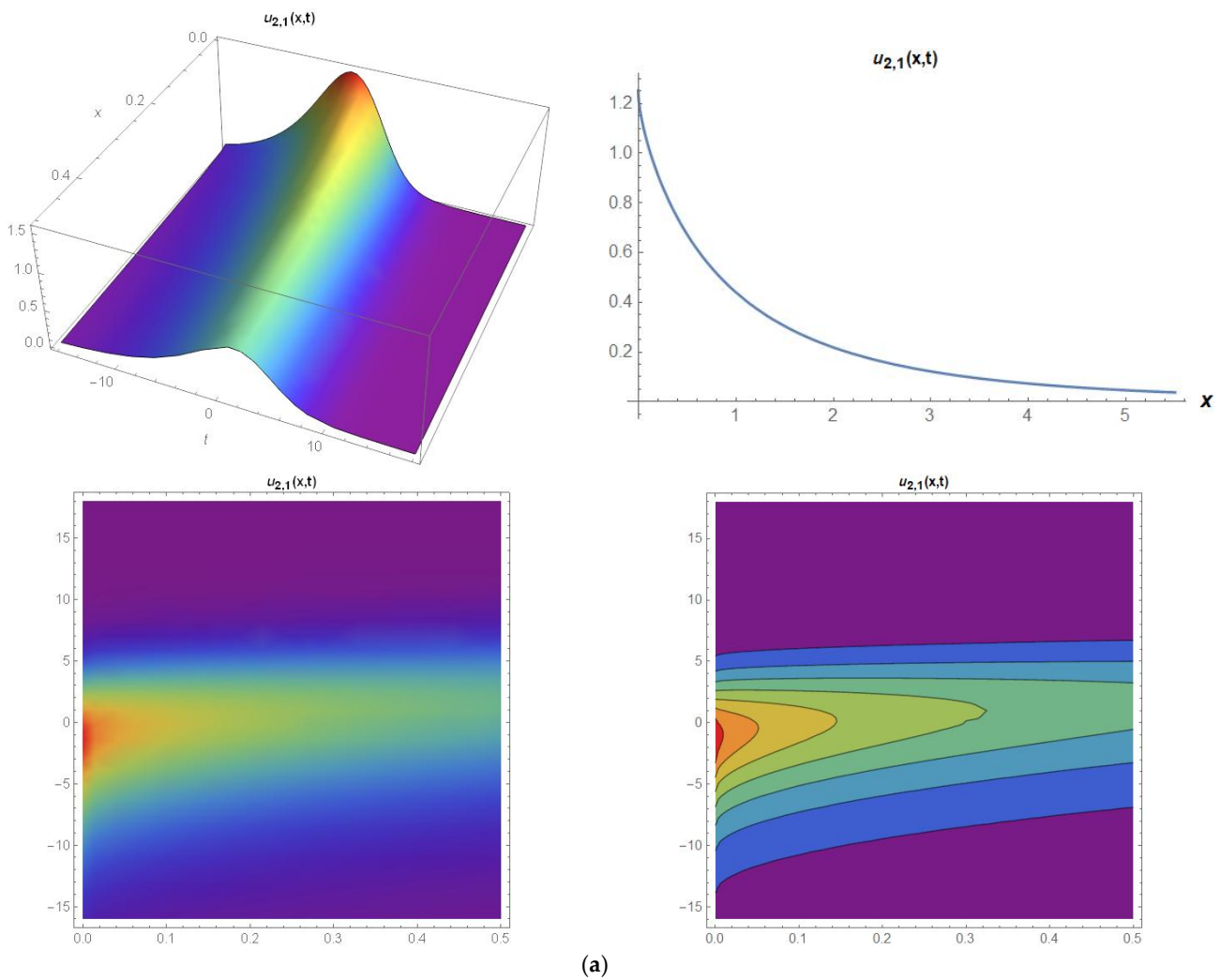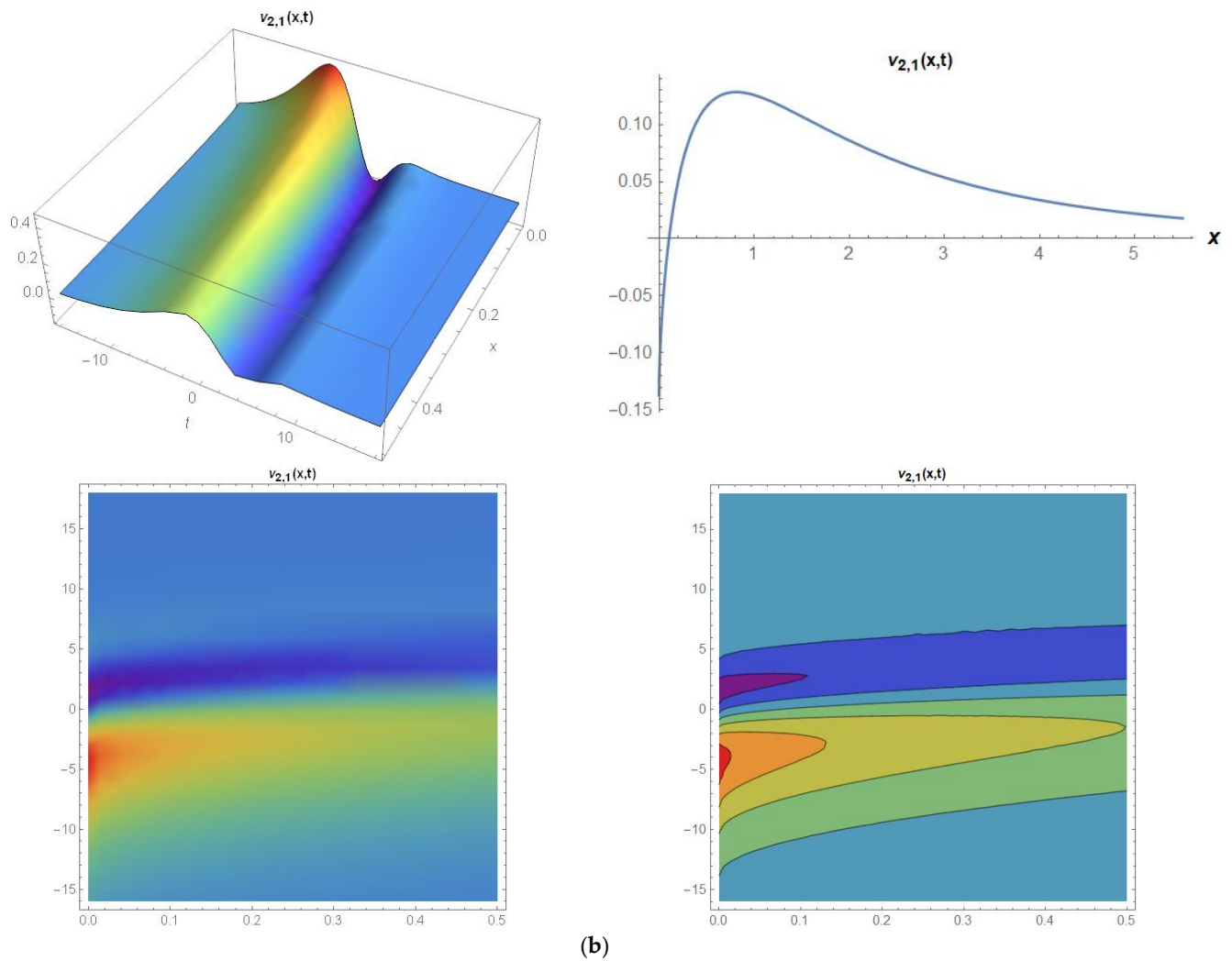

Figure 12. *Cont.*

Figure 12. (**a**) Three−dimensional, two−dimensional, density, and contour graphics of Equation (59). (**b**) Three−dimensional, two−dimensional, density, and contour graphics of Equation (60).

Figure 12a,b display the behavior of Equations (59) and (60) for the values of $a_0 = -0.413917$, $a_1 = 1.4548$, $a_2 = -1.0748$, $b_0 = 0.827834$, $b_1 = -0.76$, $\psi = -0.5$, $\sigma = 0.77$, $\Psi = 1.32$, $\alpha = 0.5$, $t = 1$.

$$u_{2,2}(x,t) = -\frac{6\sqrt{2}e^{-1/2\sigma^2 t + \sigma\,\Psi(t) + \xi}}{1 - 8e^{\xi} + 7e^{2\xi}}, \tag{61}$$

$$v_{2,2}(x,t) = \frac{3\sqrt{2}\psi e^{-1/2\sigma^2 t + \sigma\,\Psi(t)}\mathrm{csch}^2\left[\frac{\xi}{2}\right]\left(\nabla(\xi)\sinh\left[\frac{\xi}{2}\right] - 3\right)}{2(\nabla(\xi))^2}, \tag{62}$$

where $\nabla(\xi) = 4\sinh\left[\frac{\xi}{2}\right] + 3\cosh\left[\frac{\xi}{2}\right]$.

For a better understanding for the readers, the behavior of Equations (61) and (62) are graphically represented in Figures 13a and 13b, respectively.
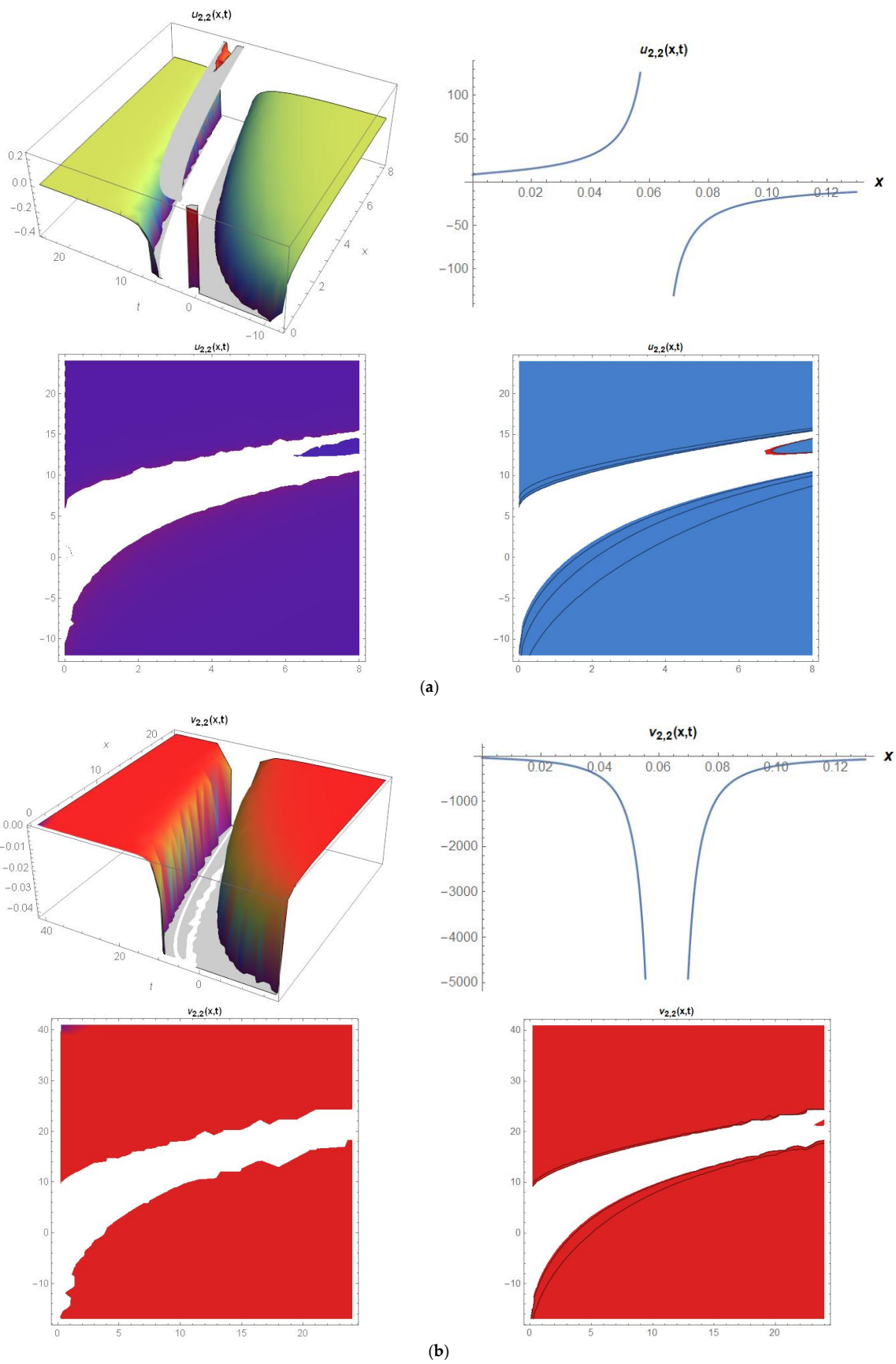
Figure 13. (**a**) Three−dimensional, two−dimensional, density, and contour graphics of Equation (61).
(**b**) Three−dimensional, two−dimensional, density, and contour graphics of Equation (62).

Figure 13a,b display the behavior of Equations (61) and (62) for the values of $a_0 = -0.413917$, $a_1 = 1.4548$, $a_2 = -1.0748$, $b_0 = 0.827834$, $b_1 = -0.76$, $\psi = -0.5$, $\sigma = 0.77$, $\Psi = 1.32$, $\alpha = 0.5$, $t = 1$.

Case 3.

$$a_0 = 0, \quad a_1 = \sqrt{2}b_1, \quad a_2 = -\sqrt{2}b_1, \quad b_0 = \frac{b_1}{6}, \quad c = -\sqrt{2}. \tag{63}$$

According to the coefficients obtained by solving the system of algebraic equations, the traveling wave solutions can be constructed as follows:

$$u_{3,1}(x,t) = \frac{3\sqrt{2}e^{-1/2\sigma^2 t + \sigma\,\Psi(t) + \xi}}{\aleph(\xi)}, \tag{64}$$

$$v_{3,1}(x,t) = -\frac{3e^{-1/2\sigma^2 t + \sigma\,\Psi(t)}\left(\sqrt{2}\,\psi\,\aleph(\xi) + 6\right)}{(\aleph(\xi))^2}, \tag{65}$$

where $\aleph(\xi) = 4 + 4\cosh[\xi] - 3\sinh[\xi]$.

For a better understanding for the readers, the behavior of Equations (64) and (65) are graphically represented in Figures 14a and 14b, respectively.
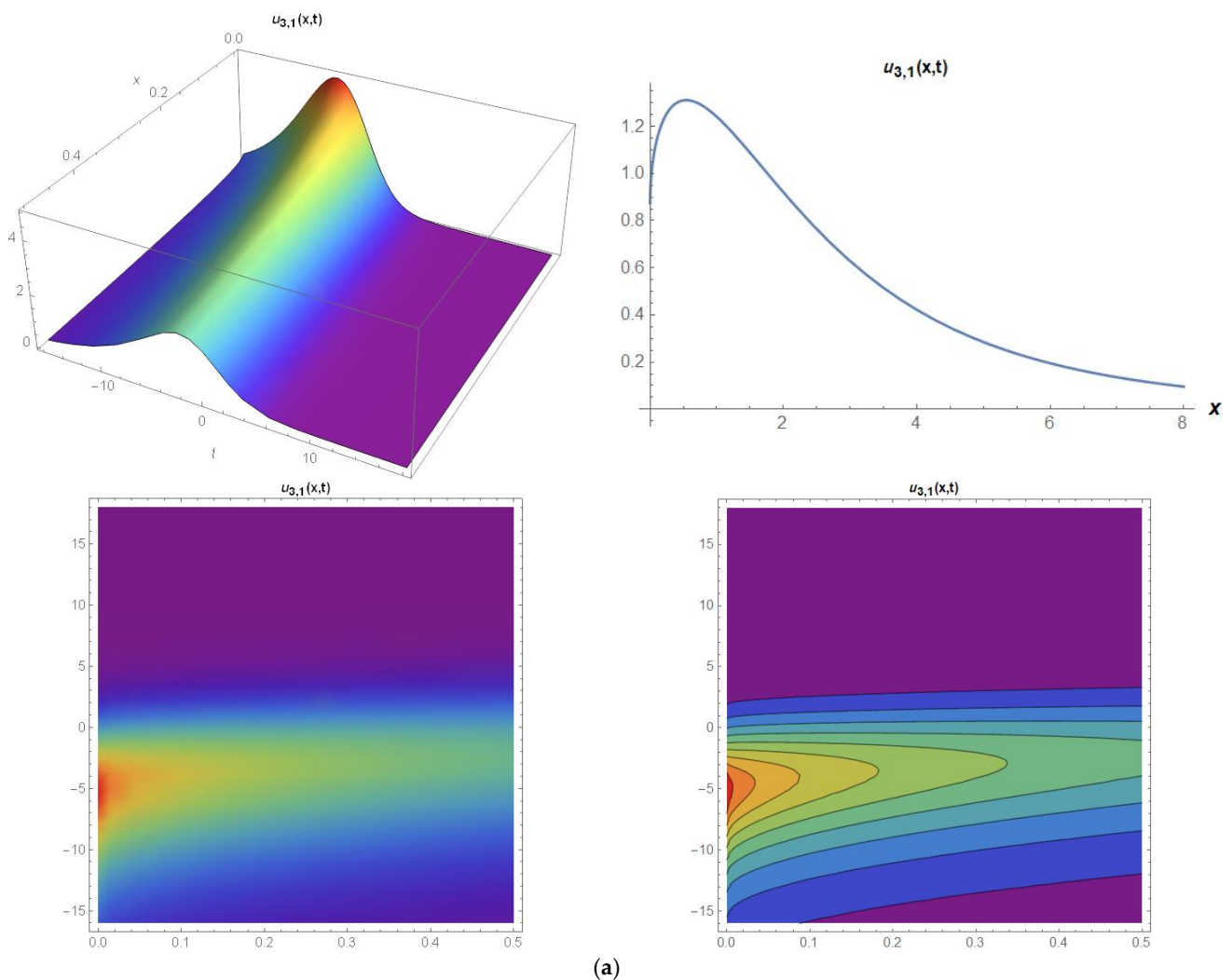

(**a**)

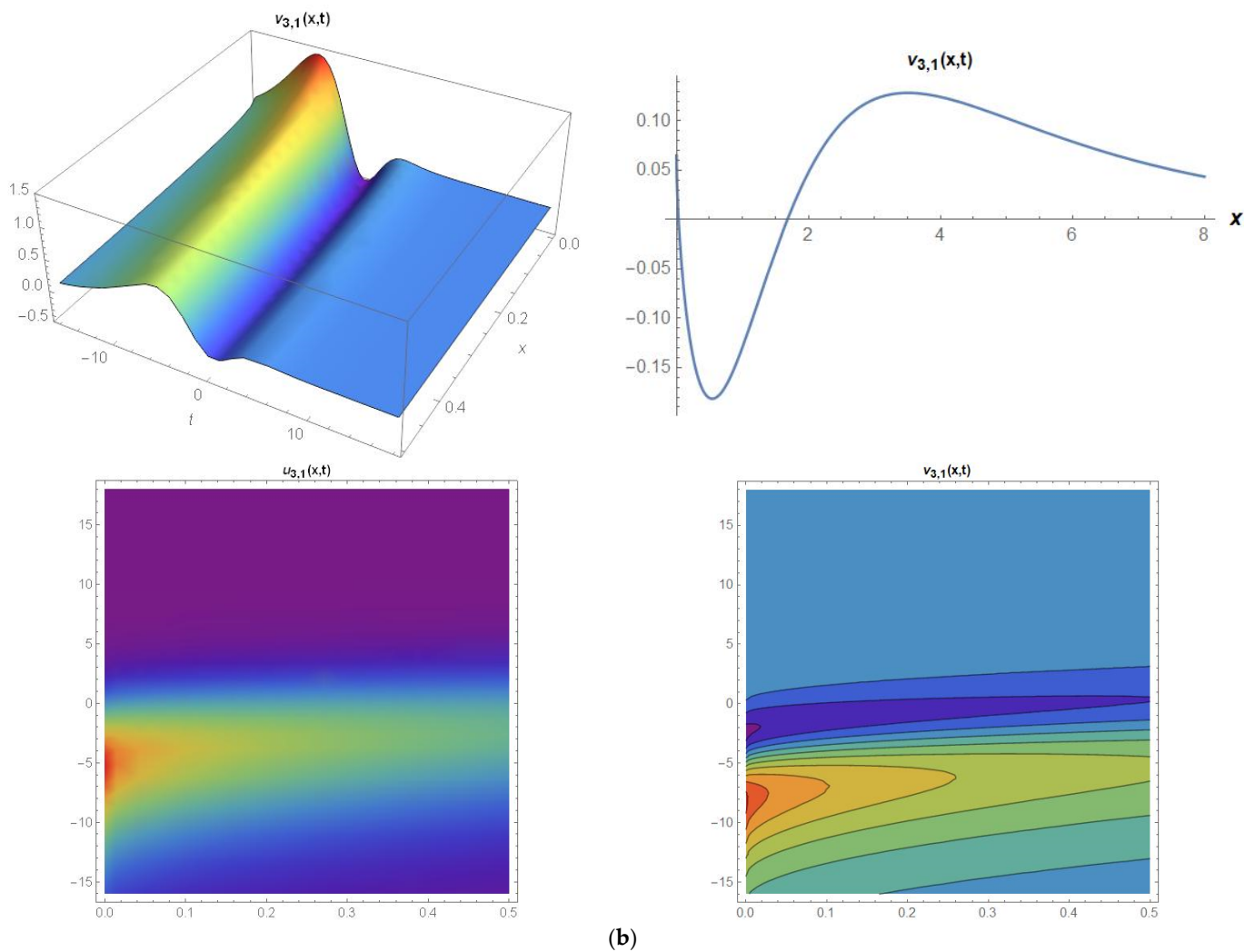**Figure 14.** *Cont.*

Figure 14. (**a**) Three−dimensional, two−dimensional, density, and contour graphics of Equation (64). (**b**) Three−dimensional, two−dimensional, density, and contour graphics of Equation (65).

Figure 14a,b display the behavior of Equations (64) and (65) for the values of $a_0 = -0.413917$, $a_1 = 1.4548$, $a_2 = -1.0748$, $b_0 = 0.827834$, $b_1 = -0.76$, $\psi = -0.5$, $\sigma = 0.77$, $\Psi = 1.32$, $\alpha = 0.5$, $t = 1$.

$$u_{3,2}(x,t) = -\frac{6\sqrt{2}e^{-1/2\sigma^2 t + \sigma\,\Psi(t) + \xi}}{7 - 8e^\xi + e^{2\xi}},$$

$$v_{3,2}(x,t) = \frac{6e^{-1/2\sigma^2 t + \sigma\,\Psi(t) + \xi}\left(7\sqrt{2}\psi - 4\left(3 + 2\sqrt{2}\psi\right)e^\xi + \sqrt{2}\psi e^{2\xi}\right)}{\left(7 - 8e^\xi + e^{2\xi}\right)^2}. \tag{66}$$

$$v_{3,2}(x,t) = \frac{6e^{-1/2\sigma^2 t + \sigma\,\Psi(t) + \xi}\left(7\sqrt{2}\psi - 4\left(3 + 2\sqrt{2}\psi\right)e^\xi + \sqrt{2}\psi e^{2\xi}\right)}{\left(7 - 8e^\xi + e^{2\xi}\right)^2} \tag{67}$$

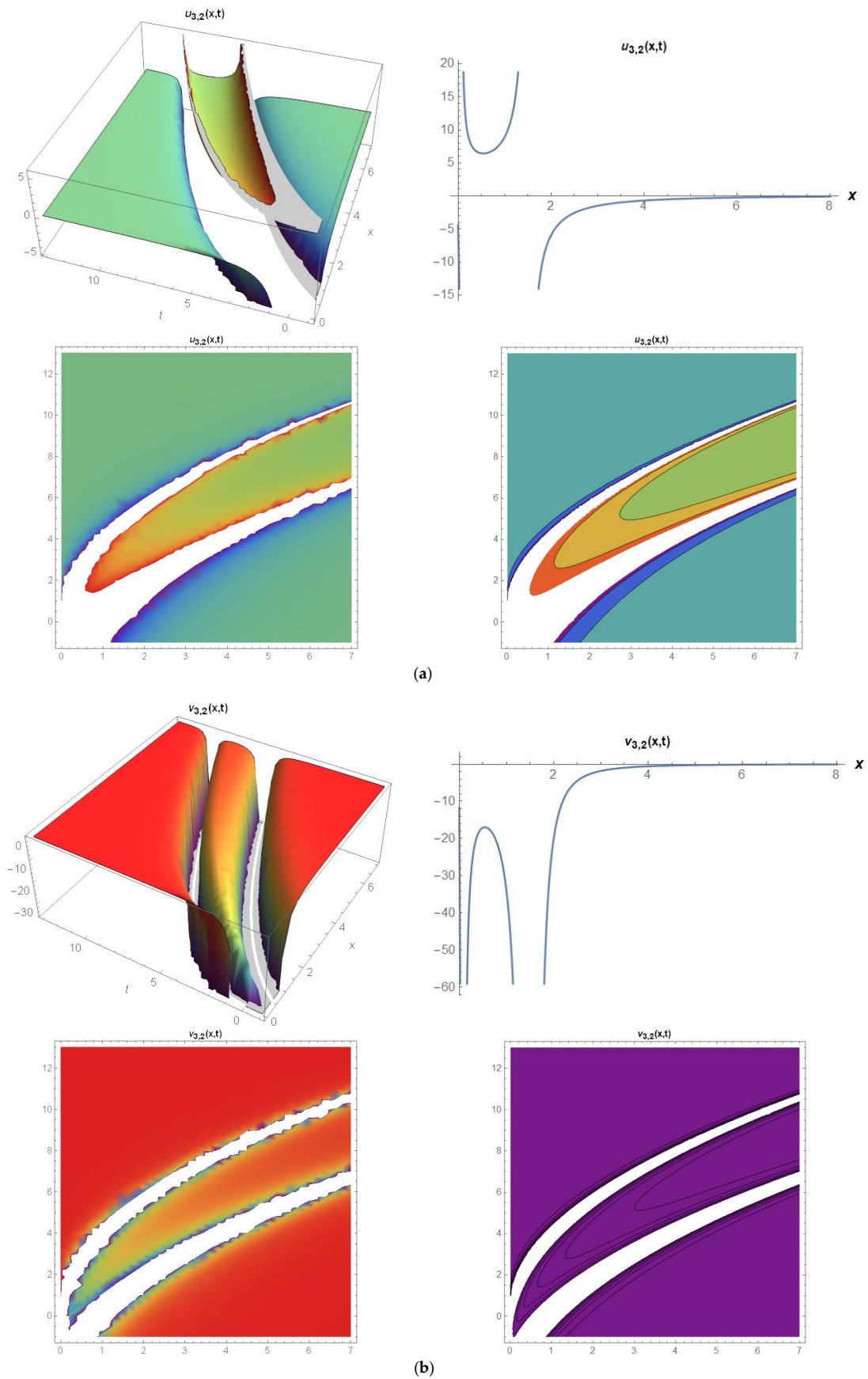The behavior of Equations (66) and (67) are graphically represented in Figures 15a and 15b, respectively.

(**a**)

(**b**)

Figure 15. (**a**) Three−dimensional, two−dimensional, density, and contour graphics of Equation (66). (**b**) Three−dimensional, two−dimensional, density, and contour graphics of Equation (67).

Figure 15a,b display the behavior of Equations (66) and (67) for the values of $a_0 = -0.413917$, $a_1 = 1.4548$, $a_2 = -1.0748$, $b_0 = 0.827834$, $b_1 = -0.76$, $\psi = -0.5$, $\sigma = 0.77$, $\Psi = 1.32$, $\alpha = 0.5$, $t = 1$.

7. Conclusions

Two different methods called the modified exponential function method, and the generalized Kudryashov method are applied to stochastic conformable Broer–Kaup equations in this study. These two methods have several advantages and disadvantages. Both methods aim to obtain solution functions with periodic function properties. Since such behavior models obtained in a range can be generalized to an infinite range, if the solution functions obtained are periodic, it will be possible to extend the behavior of the mathematical model in a certain range to a more general range. In this study, a package program called "Mathematica" was used for all mathematical operations and graphs simulating the behavior of the mathematical model in both methods and to show that the solution functions themselves provide this mathematical model. The program used in the calculations and graphic drawings in this article is a very effective program: because, with the help of this program, it is very easy to draw graphs to examine the behavior of the solutions found as well as many mathematical operations such as the parametric solutions of highly complex nonlinear algebraic equation systems; the derivatives and the integrals of functions; and also the examining of whether the solution functions provide the relevant differential equation or not. First of all, the hyperbolic, trigonometric, and rational solution functions of the mathematical model handled were obtained by the modified exponential function method. Then, similar solution functions were determined via the second method, the generalized Kudryashov method. When a comparison is made between these two methods, the fact that some solution families cannot be obtained due to the conditions and properties of the modified exponential function method and obtain some fixed solution functions can be considered as a negative behavior. On the other hand, it is seen that such a situation is not encountered in the generalized Kudryashov method. Therefore, the solution function models of the generalized Kudryashov method are more valuable because they have a helpful structure. In the near future, we aim to apply these methods to obtain the wave solutions of stochastic differential equations with beta derivatives.

Author Contributions: Conceptualization, Y.G. and H.Y.; methodology, Y.P.; software, T.A.; validation, Y.G., H.Y. and Y.P.; formal analysis, T.A.; investigation, Y.G.; writing—original draft preparation, Y.G. and Y.P.; writing—review and editing, H.Y.; visualization, T.A.; funding acquisition, H.Y. All authors have read and agreed to the published version of the manuscript.

Data Availability Statement: No data were used to support this study.

Conflicts of Interest: The authors declare no conflict of interest.

References

1. He, J.H. Comparison of homotopy perturbation method and homotopy analysis method. *Appl. Math. Comput.* **2004**, *156*, 527–539. [CrossRef]
2. Wazwaz, A.M. A reliable modification of Adomian decomposition method. *Appl. Math. Comput.* **1999**, *102*, 77–86. [CrossRef]
3. Gurefe, N.; Kocer, E.G.; Gurefe, Y. Chebyshev-Tau method for the linear Klein-Gordon equation. *Int. J. Phys. Sci.* **2012**, *7*, 5723–5728.
4. Hwang, J.H.; Lu, C.C. A semi-analytical method for analyzing the tunnel water inflow. *Tunn. Undergr. Space Technol.* **2007**, *22*, 39–46. [CrossRef]
5. Selvadurai, A.P.S. The analytical method in geomechanics. *Appl. Mech. Rev.* **2007**, *60*, 87–106. [CrossRef]

6. Djellab, N.; Boureghda, A. A moving boundary model for oxygen diffusion in a sick cell. *Comput. Methods Biomech. Biomed. Eng.* **2022**, *25*, 1402–1408. [CrossRef] [PubMed]
7. Gurefe, Y. The generalized Kudryashov method for the nonlinear fractional partial diferential equations with the beta-derivative. *Rev. Mex. Fis.* **2020**, *66*, 771–781. [CrossRef]
8. Yel, G.; Baskonus, H.M.; Bulut, H. Novel archetypes of new coupled Konno-Oono equation by using sine-Gordon expansion method. *Opt. Quantum Electron.* **2017**, *49*, 285. [CrossRef]
9. Liu, S.; Fu, Z.; Liu, S.; Zhao, Q. Jacobi elliptic function expansion method and periodic wave solutions of nonlinear wave equations. *Phys. Lett. A* **2001**, *289*, 69–74. [CrossRef]
10. Mahmud, A.A.; Tanriverdi, T.; Muhamad, K.A. Exact traveling wave solutions for (2+1)-dimensional Konopelchenko-Dubrovsky equation by using the hyperbolic trigonometric functions methods. *Int. J. Math. Comput. Eng.* **2023**, *1*, 11–24. [CrossRef]
11. He, J.H.; Abdou, M.A. New periodic solutions for nonlinear evolution equations using Exp-function method. *Chaos Soliton Fract.* **2007**, *34*, 1421–1429. [CrossRef]
12. El-Wakil, S.A.; Abdou, M.A. New exact travelling wave solutions using modified extended tanh-function method. *Chaos Soliton Fract.* **2007**, *31*, 840–852. [CrossRef]
13. Shen, G.; Sun, Y.; Xiong, Y. New travelling-wave solutions for Dodd-Bullough equation. *J. Appl. Math.* **2013**, *2013*, 364718. [CrossRef]
14. Gurefe, Y.; Pandir, Y.; Akturk, T. On the nonlinear mathematical model representing the coriolis effect. *Math. Probl. Eng.* **2022**, *2022*, 2504907. [CrossRef]
15. Attaullah; Shakeel, M.; Shah, N.A.; Chung, J.D. Modified exp-function method to find exact solutions of ionic currents along microtubules. *Mathematics* **2022**, *10*, 851. [CrossRef]
16. Pandir, Y.; Akturk, T.; Gurefe, Y.; Juya, H. The modified exponential function method for beta time fractional Biswas-Arshed equation. *Adv. Math. Phys.* **2023**, *2023*, 1091355. [CrossRef]
17. Al-Askar, F.M.; Cesarano, C.; Mohammed, W.W. Effects of the Wiener process and beta derivative on the exact solutions of the Kadomtsev-Petviashvili equation. *Axioms* **2023**, *12*, 748. [CrossRef]
18. Alshammari, S.; Mohammed, W.W.; Samura, S.K.; Faleh, S. The analytical solutions for the stochastic-fractional Broer–Kaup equations. *Math. Probl. Eng.* **2022**, *2022*, 6895875. [CrossRef]
19. Khalil, R.; Al Horani, M.; Yousef, A.; Sababheh, M. A new definition of fractional derivative. *J. Comput. Appl. Math.* **2014**, *264*, 65–70. [CrossRef]
20. Abu-Shady, M.; Kaabar, M.K. A generalized definition of the fractional derivative with applications. *Math. Probl. Eng.* **2021**, *2021*, 9444803. [CrossRef]